

pubs.acs.org/JPCB Article

# The Role of the Core Attachment Positioning in Triggering Intramolecular Singlet Exciton Fission in Perylene Diimide Tetramers

Angelar K. Muthike, Benedetta Carlotti, Ifeanyi K. Madu, Hanjie Jiang, Hyungjun Kim, Qinghe Wu, Luping Yu, Paul M. Zimmerman, and Theodore Goodson, III\*



Cite This: J. Phys. Chem. B 2021, 125, 5114-5131



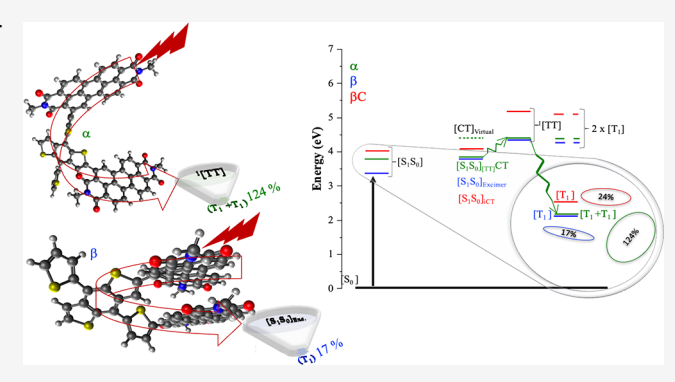
ACCESS

Metrics & More

Article Recommendations

Supporting Information

**ABSTRACT:** Previous studies have proposed that the presence of a flexible  $\pi$ -bridge linker is crucial in activating intramolecular singlet exciton fission (iSEF) in multichromophoric systems. In this study, we report the photophysical properties of three analogous perylene diimide (PDI) dendritic tetramers showing flexible/twisted  $\pi$ -bridged structures with  $\alpha$ - and  $\beta$ -substitutions and a rigid/planar structure with a  $\beta$ -fused ring ( $\beta$ C) connection to a benzodithiophene-thiophene (BDT-Th) core. The rigidity and enhanced planarity of  $\beta$ C lead to significant intramolecular charge transfer and triplet formation via an intersystem crossing pathway. Steady-state spectroscopic measurements reveal similar absorption and emission spectra for the  $\alpha$ -tetramer and the parent PDI monomer. However, their fluorescence quantum yield is



significantly different. The negligible fluorescence yield of the  $\alpha$ -tetramer (0.04%) is associated with a competitive nonradiative decay pathway. Indeed, for this twisted compound in a high polar environment, a fast and efficient iSEF with a triplet quantum yield of 124% is observed. Our results show that the  $\alpha$ -single-bond connections in the  $\alpha$  compound are capable of interrupting the coupling among the PDI units, favoring iSEF. We propose that the formation of the double triplet ( ${}^{1}[TT]$ ) state is through a superposition of singlet states known as  $[S_1S_0]_{[TT]}CT$ , which has been suggested previously for pentacene derivatives. Using steady-state and time-resolved spectroscopic experiments, we demonstrate that the conformational flexibility of the linker itself is necessary but not sufficient to allow iSEF. For the case of the other twisted tetramer,  $\beta$ , the strong  $\pi$ – $\pi$  co-facial interactions between the adjacent PDI units in its structure lead to excimer formation. These excimer states trap the singlet excitons preventing the formation of the  ${}^{1}[TT]$  state, thus inhibiting iSEF.

## I. INTRODUCTION

Singlet exciton fission (SEF) is a spin allowed process where a photogenerated singlet exciton splits into two spin-correlated triplet excitons. This mechanism has been reported to reduce thermal losses factored in the Shockley-Queisser (SQ) limit and is therefore capable of enhancing the theoretical efficiency limit of photovoltaic (PV) devices from 33 to 47%. 1-5 For SEF to occur, electronic  $(E[S_1] \ge 2(E[T_1])$  and  $E[T_2] \ge E[S_1])$  and structural (molecular packing that optimizes interchromophore electronic coupling) conditions have to be fulfilled.<sup>3</sup> There are two different mechanisms through which SEF proceeds: direct coupling where two electrons move between the singlet exciton and the adjacent ground-state chromophore to yield the correlated triplet pair state (1[TT]) or mediated through a charge transfer (CT) state where the conversion of the first singlet state ( ${}^{1}[S_{1}S_{0}]$ ) to  ${}^{1}[TT]$  is facilitated by coupling to higher-lying CT state.  $^{1,5-12}$  The formed  $^{1}$ [TT] can yield a quintet state (5[TT]) through spin evolution and/or go through spin decoherence to produce two separated triplet states  $[T_{1+} T_1]$ .

Recent studies report that the SEF mechanism can either be inter- or intramolecular. In intermolecular SEF (xSEF), the optically excited singlet state on one molecule couples with neighboring molecules to form an intermolecular triplet pair. xSEF can be improved by tuning the interchromophore interactions. This process highly depends on chromophore packing motifs. It is challenging to come up with highly ordered molecular structures to fulfil the packing requirement, and reproducibility is often an issue.<sup>13</sup> However, polymers and

 Received:
 March 20, 2021

 Revised:
 April 22, 2021

 Published:
 May 7, 2021





Figure 1. Structures of the investigated molecules and the parent PDI monomer.

other small molecules can show SF as an intrinsic property through intramolecular singlet exciton fission (iSEF) where the double triplet pair state is located on the same molecule. This iSEF mechanism, which shows high processability in solution, high tunability in both molecular and electronic structures, and ability to create tailored interfaces, is not well understood.<sup>13–15</sup>

In an effort to improve the performance of organic photovoltaics (OPVs), SEF research on structurally tunable systems of acene dimers<sup>16–31</sup> reports two main structural factors affecting the rate and yield of SF: the coupling between the molecular units and the degree of contortion in the structure.<sup>32,33</sup> Despite the great SEF yields from the aforementioned acene dimers, their limitations like photoinstability have pushed researchers to venture into new materials with SF potential.<sup>22,34,35</sup> Perylene dimides (PDIs) are a class of chromophores whose packing is easily controllable, possesses high thermal stability/photostability, has high extinction coefficients in the visible region, and holds desirable triplet energies for semiconductor sensitizaton.<sup>22,36,37</sup>

Recently, iSEF has been observed in PDI dimers and trimers. 22,32,38-40 However, Wasielewski and co-workers have observed excimer states that block the formation of the <sup>1</sup>[TT] state in solution-based aggregates of PDI dimers. 38,41-43 This excimer formation has been associated with the co-facial, slipstacked morphology of the dimers, 41 which leads to a strong electronic coupling between chromophores inhibiting SEF.4 There has been varying information about the role of excimer states in the SEF mechanism. 45-48 In some cases, excimer states inhibit the formation of the correlated triplet pair, 42,45,49,50 while in other cases, these excimer states act as intermediates for SEF. 16,47,51 The complication in understanding excimer states and their role in SEF is as a result of the indistinguishable nature of these singlet states, the  ${}^{1}[S_{1}S_{0}]$ and <sup>1</sup>[TT] states, and their interactions. <sup>45</sup> One report showed that excimers form when the electronic coupling between the CT state and the singlet excited state of two identical chromophores is strong, resulting in a stable CT + <sup>1</sup>[S<sub>1</sub>S<sub>0</sub>] mixture state, an excimer. <sup>52</sup> The individual CT state or  ${}^{1}[S_{1}S_{0}]$ can individually act to inhibit the production of double triplets from the singlet state via a highly stabilized CT (lower CT state) process or radiative decay, respectively.

Other studies have shown that, in addition to the nature of the chromophore, the  $\pi$ -linker plays a crucial role in contributing to the occurrence of iSEF in PDI chromo-

phores.<sup>40</sup> It has been reported that structural flexibility of the covalent linker is necessary to activate iSEF. <sup>19,39,40,53</sup> In our recent report, <sup>40</sup> we investigate two analogous PDI trimers where one is planar and the other one is twisted. Here, we follow up on the established work on the role and characteristics of the linker that may necessitate iSEF. While it has been established that the presence of a linker is important in triggering iSEF, this work dissects two similar structures, one with a flexible and the other one with a rigid linker. We report that the flexibility of the linker is important in activating intramolecular singlet fission since we observe a triplet yield of 170% for the flexible compound and 16% for the rigid planar compound.

In other studies, singlet fission has been reported as a solvent-dependent process for molecules like terylene diimide (TDI) dimers. S4-56 Here, SEF was observed in low dielectric constant solvents and symmetry breaking charge separation in high dielectric constant solvents. In this case, it follows that the higher dielectric constant solvent stabilizes the CT state and lowers its energy, allowing it to act as a trap state. On the other hand, minimal CT state stabilization in low dielectric environments enables the CT state to act as a virtual state in a superexchange interaction that promotes SF. On the contrary, other reports show symmetry breaking as a crucial step to activate singlet fission. Therefore, a lot of research is still needed to understand the mechanism of iSEF, the structural character of the molecules, and the appropriate dielectric environment for these molecules to show iSEF.

In this present investigation, we use time-resolved spectroscopic techniques to elucidate the crucial role of the core attachment position to the PDI units as well as the chromophore's dielectric environment in activating iSEF in PDI tetramers. Here, three analogous tetramer structures were investigated, where the PDI electron acceptor units are linked with a central benzodithiophene (BDT) electron donor moiety. The connections between the donor and the four acceptor units is realized via single bonds through the  $\alpha$  and  $\beta$  position of the PDI units for  $\alpha$ - and  $\beta$ -tetramers, respectively, for the twisted structures and through  $\beta$  ring cyclization for the planar  $\beta$ C-tetramer as shown in Figure 1.

# **II. EXPERIMENTAL METHODS**

**II.A. Materials.** The synthetic procedure of all the tetramers has been previously discussed in detail. <sup>57,58</sup> These materials

were synthesized through the Suzuki coupling between BDT-Th-4Bpin with 4 equivalents of  $\alpha$ -monobrominated and  $\beta$ -monobrominated for  $\alpha$  and  $\beta$ , respectively, while  $\beta$ C was obtained through the cyclization between the perylene diimides (PDIs) and the benzodithiophene-thiophene (BDT-Th) core of the  $\beta$ -tetramer. Chlorobenzene and toluene from Sigma-Aldrich were used as solvents for the spectral and photophysical characterization.

**II.B. Steady-State Studies.** For all our steady-state spectroscopic investigation measurements performed at room temperature and pressure, concentrations ranging from  $3.0 \times 10^{-8}$  to  $1 \times 10^{-5}$  M were used with chlorobenzene or toluene as solvents. The absorption spectra were obtained using an Agilent 8432 UV—visible absorption spectrophotometer, while a Fluoromax-2 spectrofluorimeter was used for the emission measurements. To calculate the fluorescence quantum yields of the investigated samples, a previously documented procedure was carried out  $^{59}$  and Rhodamine B in ethanol was used as the standard.  $^{60}$ 

II.C. Two-Photon Excited Fluorescence (TPEF) Studies. Our previously described mode-locked Ti:Sapphire laser, tunable from 700 to 900 nm with 110 fs pulses as an output at a repetition rate of 80 MHz, was used for our two-photon excited fluorescence measurements. The emission scans with a wavelength range of 400–850 nm were performed with an 820 nm excitation. A power dependence scan was run at the emission wavelength detection, and the highest number of counts was picked. During the TPEF measurements, a neutral density filter was used to change the input power from the laser, which would consequently vary the output intensity. Using Rhodamine B as the standard, the two-photon absorption cross section was calculated through a comparative method using the obtained two-photon power-dependent fluorescence intensity.

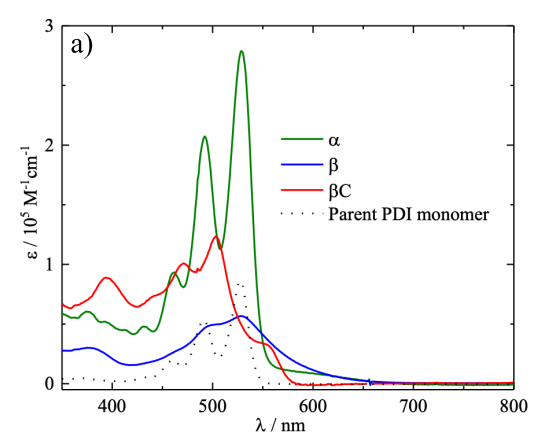
**II.D. Time-Resolved Fluorescence Studies.** The previously described time-correlated single photon counting (TCSPC) technique was used to study the long decay components of the investigated samples. A mode-locked Kapteyn-Murnane (KM) Ti-sapphire laser with an output beam at 800 nm and a pulse duration of ca. 30 fs was used for our time-resolved fluorescence measurements. A nonlinear β-barium-borate (BBO) crystal was used to double the output frequency beam to a 400 nm, and a polarizer was used to vary the power of the 400 nm sample excitation beam. During the measurements, a lens of focal length 11.5 cm was used to focus the 400 nm beam on the sample cell (quartz cuvette, 0.4 cm path length). The fluorescence was then collected perpendicularly to the incident beam into a monochromator. The output from the monochromator was coupled to a photomultiplier tube, which converted the photons into counts.

In addition to the TCSPC, an ultrafast fluorescence upconversion (FUC) setup was used to obtain the fs-resolved fluorescence measurements. For this setup, a Mode-Locked Ti-Sapphire fs laser (Spectra Physics Tsunami) pumped by a continuous 532 nm output from a Spectra Physics Millenia laser whose gain medium is a neodymium-doped yttrium vanadate (Nd:YVO<sub>4</sub>) was used. The mode-locked Ti-Sapphire generated 80 fs pulses at 800 nm, with a repetition rate of 82 MHz. Using a second-harmonic  $\beta$ -barium-borate (BBO) crystal, a 400 nm excitation beam whose power ranged between 33 and 35 mW was generated and the 800 nm residual propagated through a computer-controlled motorized optical delay line. The beam polarization was achieved using a

Berek compensator. The sample fluorescence emission was then up-converted by a nonlinear BBO crystal using the 800 nm residual beam previously delayed by the optical delay line with a gate step of 6.25 fs. A monochromator was used to select the wavelength of the up-converted beam of interest, which is then detected using a photomultiplier tube (Hamamatsu R152P) converting the detected beam into computer-readable photon counts. To calibrate this setup, Coumarin 30 was used while a water Raman signal was used to determine the instrument response function to have a width of 110 fs.

II.E. Femtosecond Transient Absorption. A Spectra Physics Spitfire amplified laser system previously described<sup>61</sup> was used for the femtosecond transient absorption (fsTA) measurements. The produced beam of ~100 fs pulse duration, 1 kHz repetition rate, and a power of 1 W was directed at a beam splitter to generate the pump (85%) and the probe beam (15%). The 510 nm to 66 mJ per pulse pump beam was focused onto the sample cell (l = 2 mm), which is preceded by an optical chopper. On the other hand, the probe beam was passed through a computer-controlled delay line and focused onto a 2 mm sapphire plate to generate the white light continuum (Helios by Ultrafast Systems Inc.). This white light was then focused onto the sample where it overlapped with the pump beam. An Ocean Optics charge-coupled device (CCD) detector collected the difference in the signal absorbance  $(\Delta A)$ . The Helios software by Ultrafast Systems Inc. was used for the transient data acquisition, while the data analysis was completed using Surface Explorer Pro and Glotaran software.

II.F. Nanosecond Transient Absorption. The nanosecond transient absorption (nsTA) setup was used to probe the spectral, emissive, and non-emissive lifetimes of long-lived transient species of the investigated chromophores as described earlier.<sup>61–63</sup> A Spectra Physics QuantaRay neodymium-doped yttrium aluminum (Nd:YAG) nanosecond laser coupled with a GWU Optical Parametric Oscillator (OPO) with wavelength tunability ranging between 250 and 2600 nm was used as the pump excitation source. A highenergy Q-Switched 355 nm beam from the Nd:YAG's third harmonic was used to pump the OPO, which, through second harmonic generation and sum frequency mixing (with 1064 nm) nonlinear processes, can be used to produce the long range of pump wavelengths. An LP980 Edinburg spectrometer system houses the probe source, the sample chamber, and the monochromator. The probe source is a 150 W ozone-free xenon lamp that produces a continuous 6 ms pulse with a wavelength range of 190-2600 nm. The laser pump beam excites the sample perpendicular to the probe beam, creating the transient species. The absorption properties of the produced excited states are then probed using the xenon probe source. The resultant sample light is focused to the monochromator and detected by a photomultiplier tube (PMT) (Hamamatsu R928) whose detection ranges from 185 to 870 nm. The PMT converts the obtained transmission to electric signals, which can be measured by our TDS3052B oscilloscope and converted from volts to change in absorption  $(\Delta A)$  using the L900 software supplied by Edinburg. Measurements were performed in diluted aerated and deaerated solutions of 10<sup>-5</sup> M concentrations, and photodegradation was checked by recording UV-vis absorption spectra before and after the experiments. For this investigation, 415, 510, and 594 nm excitation wavelengths were used to pump the samples. The experimental setup was calibrated by



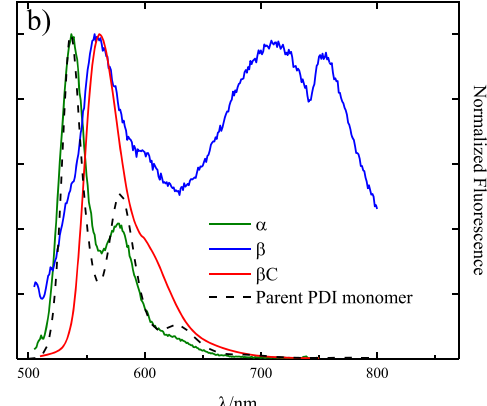


Figure 2. Absorption (a) and normalized emission (b) spectra of the tetramers in chlorobenzene. Spectra of the parent PDI monomer are also included.

an optically matched solution of tetracene ( $\phi_T$  = 0.62 and  $\varepsilon_T$  = 31,200 M<sup>-1</sup> cm<sup>-1</sup> at the corresponding absorption maximum of 465 nm)<sup>64</sup> in chlorobenzene. Triplet–triplet absorption coefficients ( $\varepsilon_T$ ) were determined by energy transfer from  $\beta/\beta C$  to tetracene and from 5,10,15,20-tetraphenyl-21*H*,23*H*-porphine in chlorobenzene ( $\varepsilon_T$  = 6000 M<sup>-1</sup> cm<sup>-1</sup> at  $\lambda_{max}$  = 790 nm) to  $\alpha$  by using a procedure previously detailed by Carlotti et al. <sup>40,64</sup>

II.G. Quantum Chemical Calculations. The theoretical investigations were performed on the molecular structures where the long alkyl chains were replaced by short chains (propyl and hexyl groups [C<sub>3</sub>H<sub>7</sub> and C<sub>6</sub>H<sub>13</sub>] attached to the perylene diimide (PDI) while the benzodithiophene (BDT) linkers were replaced by hydrogen atoms and methyl groups, respectively) to save computational time without a significant effect on the electronic properties. The ground-state geometry of each compound was obtained by density functional theory (DFT), using the long-range corrected wB97X-D functional<sup>65,66</sup> and the 6-31G\* basis set. Optimization of the lowest energy triplet state [T<sub>1</sub>] was performed using unrestricted DFT, and the ground state [S<sub>0</sub>] was performed using the restricted DFT. Excited-state simulations were performed using time-dependent DFT (TD-DFT). Singlepoint energy calculations were done using  $\omega$ B97X-D, 65,66 the 6-31G\* basis set, and the polarizable continuum model (PCM)<sup>67</sup> with a dielectric constant of 5.62 for chlorobenzene and 2.38 for toluene. Characters of excitations were described with natural transition orbitals (NTOs).

Restricted active space spin flip (RAS-SF) methods were used to provide relative energies of all double-triplet states and identify the differences between the multiexcitonic states in the three tetramers. To perform RAS-SF calculations for molecules with such large sizes, RAS-SF was performed on the "half" tetramers with only 2 PDI units. To obtain these "half" tetramers, all the molecules were truncated through the benzodithiophene (BDT) core where one of the two remaining PDI units is connected to one end of the BDT core while the other PDI unit is connected to the adjacent thiophene. Through the truncations of  $\alpha$ ,  $\beta$ , and  $\beta$ C, respective Dimer- $\alpha$ , Dimer- $\beta$ , and Dimer- $\beta$ C were obtained and used in the RAS-SF calculations. Because RAS-SF tends to overestimate the excitation energies, the absolute excitation energy values are in poor agreement with TD-DFT. Regardless, RAS-SF does provide trends and relative energy values (especially

for double triplet states) that cannot be realized by any other methods.

The driving force of singlet fission, i.e.,  $\Delta E_{\rm SF} = 2 \times E[T_1] - E[S_1]$ , was estimated with the methods just mentioned. Recently, multiple researchers have pointed out the importance of  $^1[{\rm TT}]$  energy in predicting the feasibility of SF and relevant kinetics.  $^{19,26,45,47}$  Amongst the various chromophores of this study, the truncated tetrameric PDI chromophores, Dimer- $\alpha$ , Dimer- $\beta$ , and Dimer- $\beta C$ , with the restricted active space double spin-flip method, which has successfully provided useful characterization of ground and excited radical states in a number of studies.  $^{68-72}$  All the calculations were performed using the Q-Chem 5.0 software package. Natural transition orbitals (NTOs) of TD-DFT calculations were visualized using IQMOL. Natural orbitals (NOs) of RAS-2SF calculations were plotted using Molden, Visual Molecular Dynamics (VMD), and POV-ray.

#### III. RESULTS

III.A. Steady-State and Nonlinear Optical Properties. Shown in Figure 2 and Figure S1 are the steady-state absorption and emission spectra for the investigated tetramers as well as those for the parent PDI monomer. For the  $\alpha$  and  $\beta$ compounds, the strongest absorption peaks, both of which are around 529 nm, have been assigned to 0-0 transitions. For both of these compounds, the peaks located around 492 and 461 nm were assigned to 0-1 and 0-2 transitions, respectively. 57,58 For the  $\beta$ C, the absorption peaks at 554, 503, and 471 nm are assigned to 0-0, 0-1, and 0-2 transitions, respectively. For this chromophore, the 0-1 and 0-2 transitions have been associated to the absorption of perylene diimide-thiophene (PDI-Th) while the 0-0 transition peak is from the absorption of perylene diimide-benzodithiophene-perylene diimide (PDI-BDT-PDI).58 The absorption and emission spectra of the  $\alpha$  chromophore in chlorobenzene are nearly identical to those of the parent PDI monomer (Figure 2 and Figure S1). This similarity indicates minimal ground-state interaction/excitonic coupling among the chromophores. 58,76,77 In addition, it suggests that the excitation is mainly localized on one of the PDIs in this  $\alpha$ -tetramer. At the 0–0 transitions, the extinction coefficient of  $\alpha$  (~290,000 M<sup>-1</sup> cm<sup>-1</sup>) is approximately four times that of the parent PDI monomer ( $\sim$ 85,000 M<sup>-1</sup> cm<sup>-1</sup>). A similar trend is observed in the other transitions in the visible part of the spectrum.<sup>77</sup> This suggests that the extinction coefficient of  $\alpha$  is the same as that

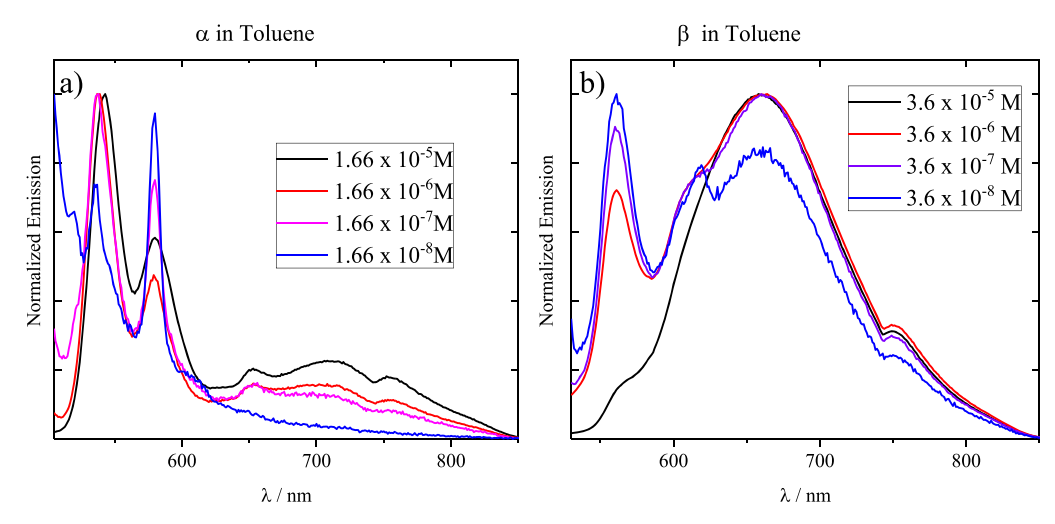


Figure 3. Concentration effect on the emission spectra of  $\alpha$  (a) and  $\beta$  (b) tetramers in toluene.

Table 1. Linear and Nonlinear Optical Properties for the Tetramers in Chlorobenzene (and Toluene for the  $\phi_F$  (%) $^e$ )

compound	$\lambda_{\rm abs} \ ({\rm nm})$	$\lambda_{em}$ (nm)	Stokes shift (cm <sup>-1</sup> )	$\varepsilon \left( \mathbf{M}^{-1} \ \mathbf{cm}^{-1} \right)^{d}$	$\phi_{ extsf{F}}\left(\% ight)$	$\phi_{\mathrm{F}}\left(\%\right)^{e}$	$\delta_{\text{TPA}}/\text{GM} \ \lambda_{\text{exc}}$ = 820 nm
PDI monomer	461, 492, <u>529</u>	537, 578	282	85700 <sup>a</sup>	~88 <sup>b</sup>	97	1 <sup>c</sup>
$\alpha$	461, 492, <u>529</u>	<u>537</u> , 578 <sup>(sh)</sup>	282	289500	0.04	1.3	71.1
β	499, <u>529</u>	562, 710	1110	59200	0.4	2.7	30.5
$\beta$ C	471, <u>503</u> , 554	562, 603 <sup>(sh)</sup>	257	131100	7.2	22.5	234
<sup>a</sup> See ref. <sup>35</sup> <sup>b</sup> See ref. <sup>40</sup> <sup>c</sup> See ref. <sup>79</sup> <sup>d</sup> At the underlined maximum wavelength. <sup>e</sup> In toluene as a solvent.							

of the parent PDI monomer given that the  $\alpha$ -tetramer is made up of four PDI units (Figure 2). The structured spectra of  $\beta$ C reflect its molecular rigidity. However, less structured absorption and emission spectra are observed for  $\beta$ . These observations are consistent with the chromophore's increased flexibility and interchromophore coupling relative to  $\alpha$  and  $\beta$ C. The emission spectrum of  $\beta$  shows a narrow band peaked around 560 nm and an additional broad and red-shifted band at 710 nm. The absorption maximum wavelength for  $\alpha$  and  $\beta$ (530 nm) is similar to that of the parent PDI monomer, The  $\beta$ C absorption maxima is similar to that of a benzodithiophene (BDT) substitute. <sup>78</sup> Therefore, the  $\alpha$ - and  $\beta$ -substitutions favor the PDI acceptor absorption while the ring fusion favors the BDT donor absorption. Additionally,  $\beta$ 's absorption wavelength is the most red-shifted, followed by  $\alpha$ , while  $\beta$ C has the most blue-shifted absorption wavelength. Additionally, it has been reported that when the  $\pi$ -bridge of a PDI derivative is a rigid cyclized aromatic ring, the spectra appear narrower, structured, and blue-shifted, which is the case for  $\beta$ C.<sup>40</sup>

The probability of aggregation was considered by investigating the concentration dependence of the absorption spectra. No concentration effect was observed on the absorption spectra of all the investigated tetramers (Figure S2A) in the range of concentrations of  $6 \times 10^{-7}$  to  $1 \times 10^{-5}$  M employed in this work. For  $\beta$ C compounds in chlorobenzene, there was no dependence of the emission spectra on the sample concentration (Figure S2). However,  $\alpha$  shows an inconsistent dependence of emission on concentration, which happens to the monomer peaks (Figure 2B). Interestingly, the significant spectral changes revealed upon increasing the  $\beta$ concentration in chlorobenzene are associated with the formation of excimers.<sup>58</sup> These excimers explain the characteristic shape of the emission spectrum of  $\beta$ , which shows both the monomer (at 560 nm) and the excimer (at 710 nm) contributions (Figure 2b). The absorption and the emission of  $\beta$  and  $\beta$ C in a less polar solvent (toluene as shown in Figure S1) are similar to those measured in chlorobenzene. However, the emission spectrum of  $\alpha$  in toluene had an additional band near 700 nm (Figure S1), indicating the presence of excimers. The investigation of the concentration effect on the emission in toluene thus confirms the formation of excimers for both  $\alpha$  and  $\beta$  in toluene (Figure 3).

The fluorescence efficiency of all the investigated compounds was measured in chlorobenzene. We found values of 0.04%, 0.4%, and 7.2% for  $\alpha$ -,  $\beta$ -, and  $\beta$ C-tetramers, respectively (see Table 1). These quantum yields are smaller in comparison to that of the parent PDI monomer  $(\sim 100\%)$ ,  $^{40,77}$  particularly observed in the case of the flexible compounds. The fluorescence quantum yields for the tetramers are similar to the previously reported quantum yields of similarly linked PDI trimers.  $^{40}$  The significantly small fluorescence quantum yield observed for the  $\alpha$  compound in comparison to that of the parent PDI monomer, whose absorption spectra is very similar to that of  $\alpha$ , indicates the presence of a non-radiative process and has been associated with reduced oscillator strength as well as low torsional activation barrier. In toluene, fluorescence quantum yields for all the investigated molecules generally increase (by two orders of magnitude for  $\alpha$  and an order of magnitude  $\beta$ - and  $\beta$ Ctetramers). It is clear that  $\alpha$ 's quantum yield increases significantly in toluene. In fact, the fluorescence quantum yield of  $\alpha$  in toluene is similar to that of  $\beta$  in toluene. This similarity shows that, in toluene, both  $\alpha$  and  $\beta$  have similar photophysical properties and substantiates the formation of excimer states for  $\alpha$  in toluene.

The two-photon absorption (TPA) cross sections show remarkable values of tens and hundreds of GM (see Table 1 and Figure S3). The TPA cross section for the  $\alpha$  compound is more than one order of magnitude bigger than that reported for the parent PDI molecule. It is also clear that the TPA cross

sections are enhanced by over one order of magnitude for the rigid  $\beta$ C (ca. 234 GM) with respect to the flexible  $\alpha$  and  $\beta$  (ca. 30–71 GM). Increased TPA cross section has been associated with an increase in transition dipole moments, which is directly proportional to the charge transfer character of the transition. Therefore, the increased TPA absorption cross section of the rigid, fused ring connected molecule indicates its higher intramolecular charge transfer (iCT) character in the excited state with respect to the flexible, single-bond bridged analogues. In addition, the higher TPA cross section observed in  $\alpha$  compared to the parent PDI monomer shows a significant increase in transition dipole moments for  $\alpha$  and hence increased iCT.

**III.B. Time-Resolved Fluorescence.** Fluorescence kinetics were acquired by both fluorescence up-conversion (FUC) and time-correlated single photon counting (TCSPC) with femtosecond and nanosecond resolution, respectively. Concentrations of  $4 \times 10^{-5}$  M,  $2.0 \times 10^{-4}$  M, and  $8.0 \times 10^{-5}$  M for  $\alpha$ ,  $\beta$ , and  $\beta$ C, respectively, were used for FUC, while  $2 \times 10^{-6}$  M,  $8.0 \times 10^{-6}$  M, and  $4.0 \times 10^{-6}$  M for  $\alpha$ ,  $\beta$ , and  $\beta$ C, respectively, were used for TCSPC measurements. From our FUC measurements, we obtained different decay lifetimes (Figure S4 and Table 2). The fast decay times can be associated with

Table 2. Lifetimes ( $\tau$ ) Obtained by Fitting the FUC Kinetics

compound	$\tau_{FUC,1}~(ps)$	$\tau_{FUC,2}$ (ps)	$ au_{ ext{FUC,3}}  ext{ (ps)}$
$\alpha$	1.2	2.6	
β	2.0	26	very long-lived component
$\beta$ C	18	130	long-lived component

the decay of the singlet-associated species back to the ground state. The  $\alpha$  compound decays to zero very fast, and therefore, only two components were applied during the data analysis. However, three components were employed for both  $\beta$  and  $\beta$ C compounds. In the  $\beta$  compound, a very long-lived component, whose lifetime could not be captured by our software, was observed. A similar component was also observed for the  $\beta$ C compound as shown in Figure S4.

To gain more insights into these long components, more fluorescence measurements were carried out using our TCSPC technique. For the rigid  $\beta$ C, these experiments revealed a lifetime of 2.64 ns at 538 nm and 2.68 ns at 562 nm (Figure S5 and Table 3). Therefore, the long-lived component observed

Table 3. Fluorescence Lifetimes Obtained by Fitting the SPC Kinetics Acquired at Different Emission Wavelength for the Tetramers in Chlorobenzene

α		β		βC	
$\lambda_{\rm em} \ (\rm nm)$	τ (ns)	$\lambda_{\rm em}$ (nm)	τ (ns)	$\lambda_{\rm em}$ (nm)	τ (ns)
538	3.68	538	3.77	538	2.64
578	3.69	560 710	3.30 2.91	562	2.68

for the  $\beta$ C compound using the FUC measurements has a decay time of about 2.7 ns. This decay time is expected to be seen as an infinite component using our femtosecond transient absorption (fsTA) measurements, which can only measure lifetimes up to 1.6 ns. For the  $\beta$  compound, we observed a fluorescence lifetime of 3.77, 3.30, and 2.91 ns at 538, 560, and 710 nm, respectively. Therefore, the lifetime of the long-lived component (3.30 ns) observed for this  $\beta$  compound using the

FUC measurements is assigned to the singlet decay lifetime. For this  $\beta$  compound, the emission wavelength effect on the fluorescence decay lifetime is consistent with the presence of different emissive species due to excimer formation for  $\beta$  in chlorobenzene. For  $\alpha$ , the fluorescence lifetime of 3.68 ns at 538 nm and 3.69 ns at 578 nm is significantly longer than the 3 ps obtained for S<sub>1</sub> decay using the FUC (Table 2) studies. In comparison to  $\beta$  and  $\beta$ C,  $\alpha$  has a longer decay time observed using the TCSPC measurements. The ca. 3.69 ns decay lifetime measured for  $\alpha$  in chlorobenzene may be due to fluorescence (either direct or delayed) associated with the double triplet excited-state  $^{1}[TT]^{80,81}$  intermediate of intramolecular singlet exciton fission (iSEF).

III.C. Femtosecond Transient Absorption. The ultrafast excited-state dynamics were investigated by femtosecond transient absorption (fsTA) using concentrations of 3.0 ×  $10^{-5}$ ,  $3.0 \times 10^{-5}$ , and  $2.0 \times 10^{-5}$  M for  $\alpha$ ,  $\beta$ , and  $\beta$ C, respectively. The time-resolved spectra (Figure 4) show positive excited-state absorption (ESA) at 740 nm and around 560 nm and negative ground-state bleaching (GSB) signals at earlier wavelengths. We also observe strong modulations in wavelengths beyond 600 nm, which are due to the instability of the white light used as the probe and does not affect the excited-state dynamics of the investigated molecules. The ESA at 740 nm has been previously associated with the perylene diimide (PDI) anion, 82-87 whereas signals between 550 and 600 nm have been assigned to the PDI cation. 83,85,86,88 For these molecules, the PDI cationic absorption band may be convoluted with GSB or triplet absorption signals and the anionic band convoluted with the  $S_n \leftarrow \overline{S}_1$  signal, as a result of spectral overlap. Global analysis of the fsTA spectra shows the presence of several exponential components as shown in Figure 5. At short delays after excitation, we observe fast components in all the investigated molecules (black and red in Figure 5). The species-associated spectra (SAS) of these fast components are similar to the SAS of the "longer" living component (blue spectra in Figure 5). This result suggests that the associated dynamics reflects the relaxation processes occurring within the same electronic excited state, the singlet state. Previous reports have mentioned the possibility of a singlet excited state with iCT character forming very fast (within solvation).89 Therefore, these two (black and red in Figure 5) fast components can be associated to the decay of the first singlet state to form a singlet solvation-relaxed state. This state relaxes further to form a final relaxed S<sub>1</sub> state. This is proposed to be a charge transfer (CT)-related state from a superposition of the singlet states known as  $[S_1S_0]_{[TT]}CT$  for  $\alpha$ , an excimer state  $([S_1S_0]_{Excimer})$ for  $\beta$ , and a CT state ([S<sub>1</sub>S<sub>0</sub>]CT) for  $\beta$ C (see Figure 5). For  $\beta$ , a CT state is not observed since the fsTA measurements were carried out in high concentrations where the excimers are the dominating species. However, the CT state with a decay of 3.30 ns was observed using TCSPC measurements where the  $\beta$ monomer was more dominant. For the  $\alpha$  compound, the component in blue leads to a subsequent formation of what is proposed to be the double triplet state, <sup>1</sup>[TT], whose decay is infinite and cannot be determined using our current fsTA due to the experimental time limit (1.6 ns). The components showing a lifetime of 160 ps for  $\alpha$ , 890 ps for  $\beta$ , and 2700 ps for  $\beta C$  represent the relaxed  $S_1$  state. At longer delays, the signal decays result in the simultaneous formation of an ESA at 510, 480, and 535 nm for the  $\alpha$ ,  $\beta$ , and  $\beta$ C respectively. The kinetics at these wavelengths exhibit a rise as shown in Figure 6, whose dynamics reported in Figure S6 match those observed

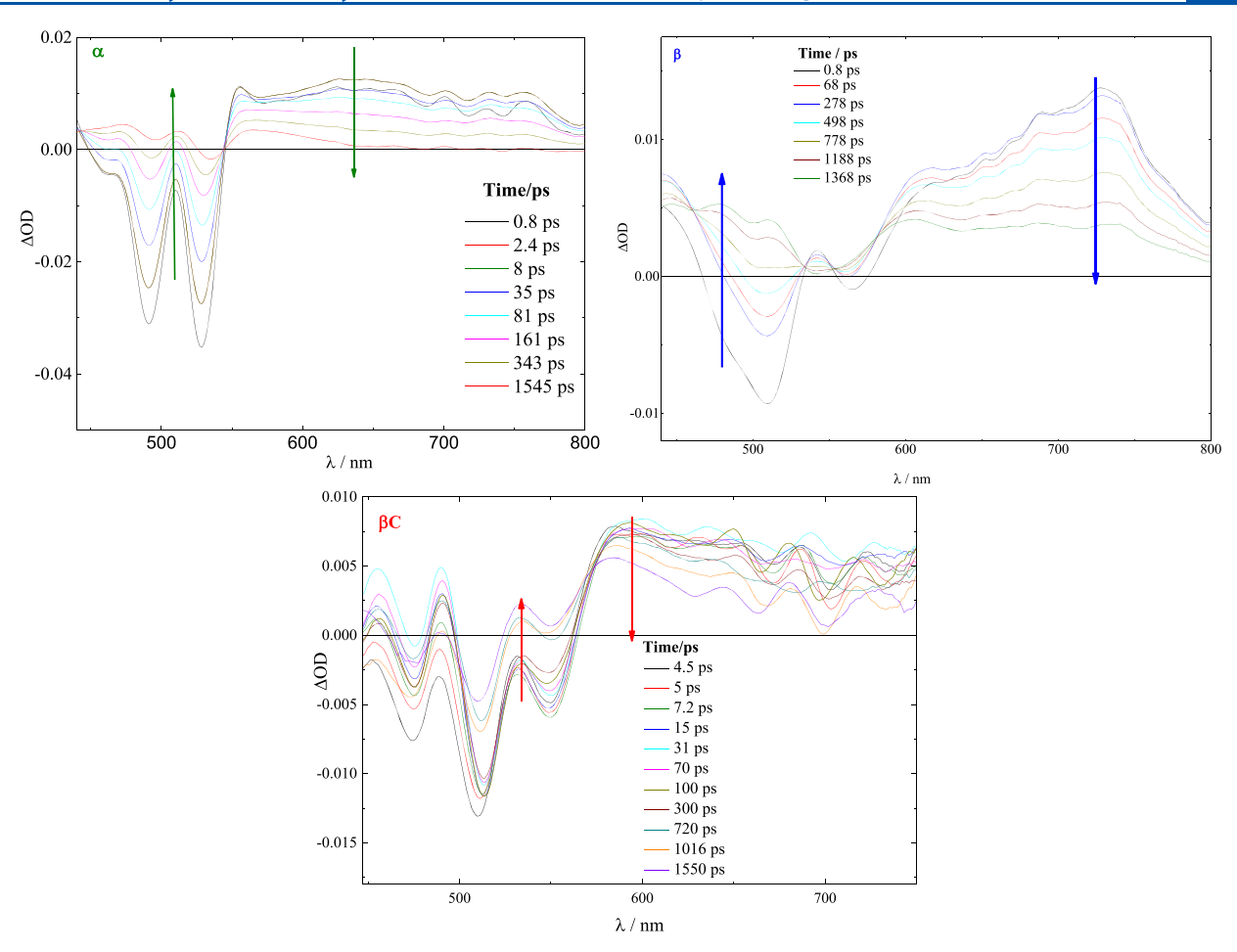


Figure 4. Femtosecond transient spectra for the investigated molecules at a 400 nm excitation in chlorobenzene.

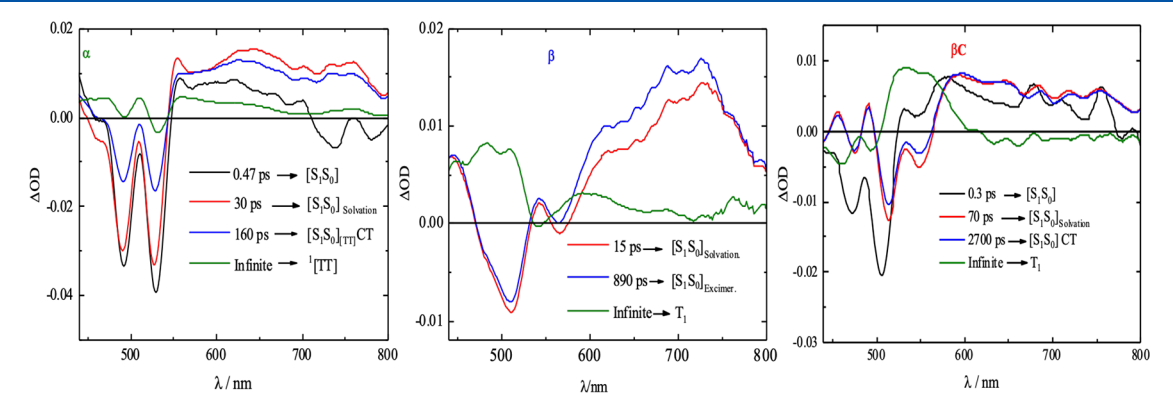


Figure 5. Species-associated spectra (SAS) and lifetimes obtained by global fitting of the fsTA data obtained using chlorobenzene as the solvent.

in Figure 5. Therefore, for the  $\beta$  and  $\beta$ C compounds, the last component (in green) represents the long-lived triplet species formed upon  $S_1$  decay and are peaked around 480–550 nm. However, for the  $\alpha$  compound, the  $[S_1S_0]_{[TT]}$ CT superposition state decays within 160 ps to form another singlet species, with both singlet and triplet characteristics, double triplet state ( $^1[TT]$ ) as shown in Figure 5. This  $^1[TT]$  state's decay lifetime is longer than our instrumental time limit and can only be assigned to infinite time using our fsTA. Therefore, for the  $\alpha$  compound, the infinite time is assigned to the decay of the precursor of triplet states,  $[T_1]$ , which happens at lifetimes longer than few nanoseconds. The fast decay of the superposition state indicates the formation of the double

triplet state, <sup>1</sup>[TT], suggesting the occurrence of singlet fission for the  $\alpha$  compound. On the other hand, for  $\beta$ , a component, which forms within 15 ps from the solvation state  $(S_1S_0]_{Solvation}$ ), decays within 890 ps, and has a singlet character, is assigned to the excimer formation  $([S_1S_0]_{Excimer})$  as shown in Figure 5. The components with infinite times are suggested to be triplet precursors' (and double triplet decay for the  $\alpha$  compound) decays since triplet decay times are longer and could not be captured due to our system time limitations. For the  $\alpha$  compound, the only tetramer whose steady-state emission spectra and triplet yields were found to be solvent-dependent, fsTA measurements were carried out in toluene. For this sample, a slower singlet decay and triplet formation

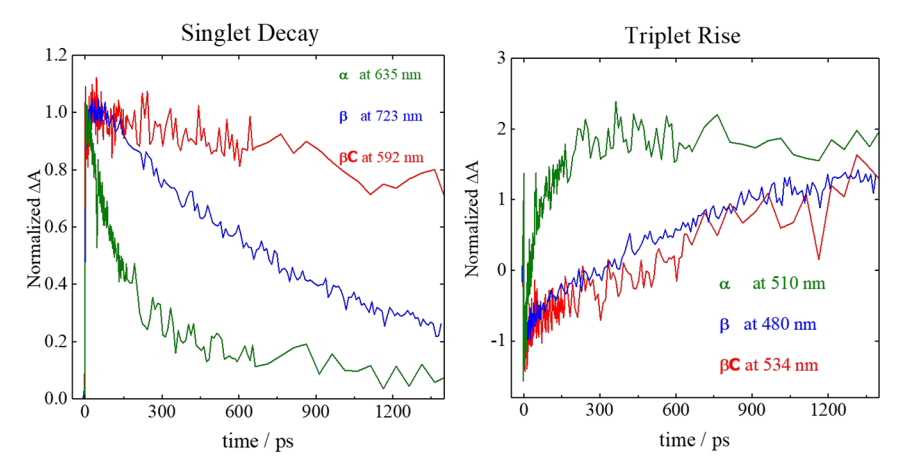


Figure 6. Femtosecond transient singlet decay (left) and triplet rise (right) kinetics for the investigated PDI tetramers in chlorobenzene.

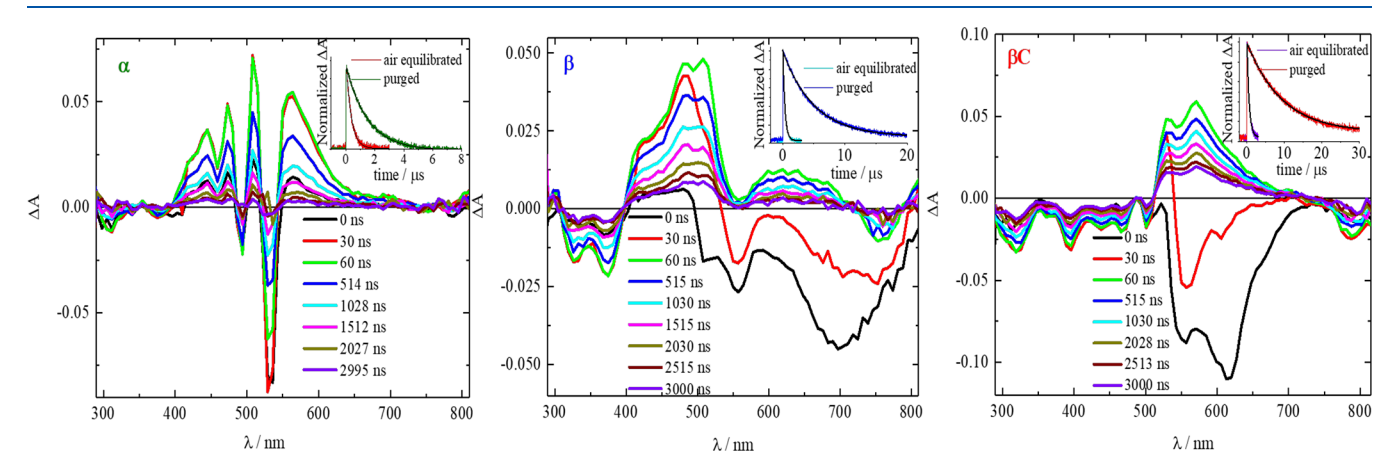


Figure 7. Nitrogen purged time-resolved spectra and triplet purged/unpurged kinetics (insets) obtained by nanosecond TA for the tetramers in chlorobenzene with a 415 nm excitation.

Table 4. Triplet Properties for the Tetramers in Chlorobenzene from Nanosecond Transient Experiments

tetramer	$\lambda_{\mathrm{T}}$ (nm)	$ au_{ m T,air}~(\mu  m s)$	$ au_{ m T,N2}~(\mu  m s)$	$\varepsilon_{\mathrm{T}}~(\mathrm{M}^{-1}~\mathrm{cm}^{-1})$	$\phi_{ ext{T}}$ chlorobenzene (average)	$\phi_{ ext{T}}$ toluene
PDI monomer <sup>a</sup>	505 <sup>a</sup>		140 <sup>a</sup>	60000 <sup>a</sup>		
$\alpha$	510	0.359	1.8	5180	1.24	0.61
β	485	0.567	8.1	12379	0.17	0.18
$\beta$ C	570	0.638	14	16029	0.24	0.09

"See ref. Triplet wavelengths, lifetimes, and extinction coefficients measurements reported here were carried out using benzene as the solvent. The triplet quantum yield of the parent PDI monomer reported in Table 4 is 0.03% in bromobenzene, 0.01% in acetonitrile, and 0.003% in benzene. 91

(380 ps) was observed relative to chlorobenzene (160 ps). This slower triplet formation could be as a result of the observed excimers in toluene.

In order to gain more insights into the mechanism of triplet production, triplet quantum yields were computed following the singular value decomposition (SVD) analysis of the fsTA results (see the Supporting Information for details on the procedure). Quantitatively related singlet and triplet ESA spectra were obtained and then used to determine the temporal population dynamics of these states. The population data (Figures S11 and S21) indicate a triplet quantum yield of 166% and 66% for  $\alpha$  and  $\beta$ C, respectively, in chlorobenzene. For the  $\alpha$  compound in toluene, the triplet yield was calculated to be 56% as shown in Figure S16. However, for the  $\beta$  compound, this calculation was inaccurate due to the spectral overlap between the GSB and triplet absorption. Even though this analysis contains many approximations, it clearly suggests

that that triplet production takes place via intramolecular singlet exciton fission (iSEF) for the  $\alpha$  and via conventional intersystem crossing (ISC) for the rigid-bridged  $\beta$ C ( $\varphi_T$  lower than 100%). Since these triplet quantum yields are mostly estimations, the nanosecond transient absorption was used to perform a rigorous experiment to accurately determine the triplet quantum yields of the investigated chromophores.

**III.D.** Nanosecond Transient Absorption. To investigate the triplet excited-state dynamics of these molecules, nanosecond transient absorption (nsTA) measurements were carried out (Figure 7) using concentrations of  $3.0 \times 10^{-6}$  M,  $8.0 \times 10^{-6}$  M, and  $5.0 \times 10^{-6}$  M for  $\alpha$ ,  $\beta$ , and  $\beta$ C, respectively. No pump wavelength dependence, solvent dependence, or spectral shift was observed for all the investigated compounds (Figure 7 and Figures S22 and S23). The nanosecond transient absorption spectra show negative signals due to ground-state bleach (GSB), as obtained in the steady-state absorption

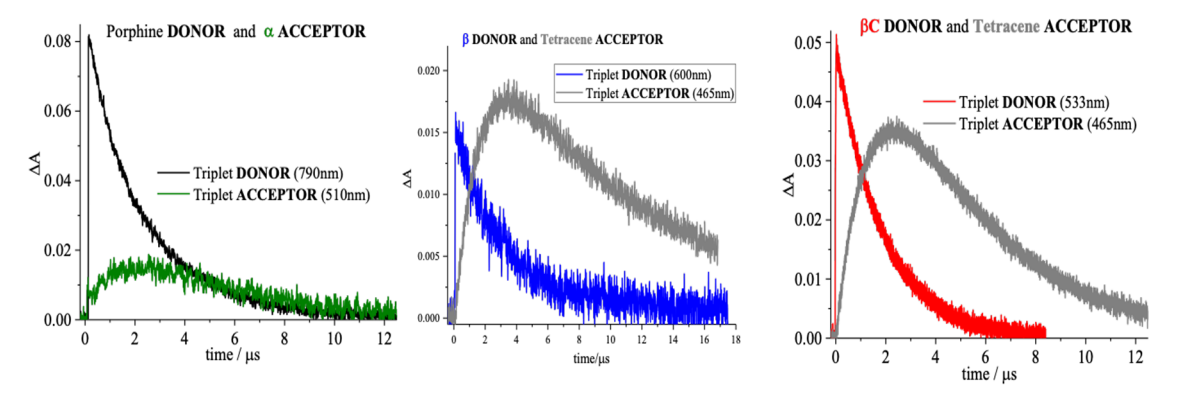


Figure 8. Decay and rise dynamics of the investigated PDI tetramers with the  $\alpha$  sensitization experiment carried out upon a 594 nm laser excitation and the  $\beta/\beta C$  sensitization experiments upon a 510 nm excitation in chlorobenzene.

spectra (Figure 2). The positive excited-state absorption (ESA) peak is centered at 510, 485, and 535 nm for the  $\alpha$ -,  $\beta$ -, and  $\beta$ C-tetramers, respectively. Signals of triplet absorption have been reported for many perylene diimide (PDI) derivatives around 500 nm. <sup>50,76</sup> Decay lifetimes of the detected transients range from hundreds of nanoseconds in air equilibrated solution to tens of microseconds in nitrogen purged solution (see Table 4). Quenching by molecular oxygen thus occur at an almost diffusional rate. Also, these transient species can be sensitized by higher triplet energy donors or are able to sensitize lower triplet energy acceptors, such as tetraphenylporphine or tetracene (Figure 8). These results allow us to assign the long-lived transients revealed by nsTA experiments to the  $T_n \leftarrow T_1$  transition of the tetramers. For the  $\beta$ - and  $\beta$ Ctetramers, negative signals due to stimulated emission were observed in the transient spectra at early delays (see the black and red spectra for  $\beta$ C in Figure 7). In addition, there was evidence of fast emission peaks centered at 556 and 700 nm for  $\beta$  and 558 and 610 nm for  $\beta$ C. These peaks are consistent with the emission peaks observed from linear emission as shown in Figure 7. The fast and broad emission peak observed for the  $\beta$ compound can be associated with the formation of excimer states. Interestingly, there were additional negative peaks observed at longer delays after excitation for both  $\beta$ - and  $\beta$ Ctetramers. For the  $\beta$ C compound, these kinetics reveal increased decay lifetimes in purged solutions relative to the unpurged solutions (Figure S24). The negative signals observed around 750 nm for  $\beta$  and 800 nm for  $\beta$ C, respectively, are attributed to phosphorescence. However, no phosphorescence was detected for  $\alpha$ , as shown in the spectra in Figure 7, suggesting a lower energetic triplet emitting in the infrared in this case.

Triplet energy transfer measurements and relative actinometry were used to accurately evaluate the triplet extinction coefficients and the triplet yields, respectively. Important information about triplet energies was also obtained from the sensitization experiments. Energy transfer was observed from the triplets of  $\beta$  and  $\beta$ C to the triplet of tetracene ( $E_T=1.27$  eV), while no triplet energy transfer was observed from  $\alpha$  to tetracene, suggesting a lower triplet energy for  $\alpha$  in comparison to the other two tetramers. The triplet of  $\alpha$  could be sensitized by employing a higher triplet energy donor such as tetraphenylporphine ( $E_T=1.43$  eV). These experimental results support the feasibility of intramolecular singlet exciton fission (iSEF) occurring in  $\alpha$  and not in  $\beta$  and  $\beta$ C because a low energy triplet is required for the SF energetic condition ( $E[S_1]>2\times E[T_1]$ ) to be fulfilled. The triplets produced upon

photoexcitation of  $\alpha$  in chlorobenzene show shorter lifetimes (1.8  $\mu$ s) relative to those produced via ISC for  $\beta$  and  $\beta$ C (8.1 and 14  $\mu$ s, respectively). Also, the triplet decay lifetime of  $\alpha$ was longer (by a factor of two) when the triplets were produced by sensitization (3.7  $\mu$ s) relative to direct excitation (1.8  $\mu$ s). This is additional evidence indicating a SEF mechanism of triplet production for  $\alpha$  as there is a higher probability that the independent triplets can return to S<sub>1</sub> via triplet-triplet annihilation (TTA), resulting in the reduced lifetime. A step-by-step triplet extinction and yield calculation for the three investigated tetramers is detailed in the Supporting Information. From the calculations detailed in Section VI of the Supporting Information and the data shown in Table 2, lower triplet extinction coefficients were observed for the flexible-bridged systems in comparison to the rigidbridged system. In addition, relative actinometry measurements were coupled with the sensitization experiments (detailed in the Supporting Information) to allow for accurate calculation of the triplet quantum yields as per eq 1:

$$\frac{[\phi_{\rm T} \varepsilon_{\rm T}]_{\rm sample \; (\beta \; or \; \beta C)}}{[\phi_{\rm T} \varepsilon_{\rm T}]_{\rm ref.}} = \frac{[\Delta A]_{\rm sample \; (\beta \; or \; \beta C)}}{[\Delta A]_{\rm ref.}} \tag{1}$$

As shown in Table 4 and Table S2, lower triplet extinction coefficients were observed for the flexible-bridged systems in comparison to the rigid-bridged system. A triplet yield higher than 100% was obtained only in the case of  $\alpha$  in chlorobenzene ( $\varphi_{\rm T}=124\%$ ), suggesting that the mechanism of triplet production proceeds via iSEF for this sample, while proceeding via traditional intersystem crossing (ISC) for the other two tetramers owing to  $\varphi_{\rm T}$  of 17% and 24% for  $\beta$  and  $\beta$ C compounds, respectively. Interestingly, in the case of  $\alpha$  in toluene, a lower triplet yield (61%) was measured. However, there was no significant change in the triplet yields calculated for  $\beta$  (18%) and  $\beta$ C (9%) in toluene compared to chlorobenzene as shown in Table 4.

**III.E.** Quantum Chemical Calculations. Density functional theory (DFT) was used to optimize the geometries and obtain the dihedral angles of the investigated chromophores. The optimized structures are shown in Figure 9 with their dihedral angles shown in Figure S33. The ground-state geometries showing similar dihedral angles obtained for both  $\alpha$  and  $\beta$  reveal that both of these molecules possess a twisted structure. However,  $\beta$ C has the lowest dihedral angle and therefore, this molecule is almost planar. In  $\alpha$ , the covalent linker is connected to the perylene diimide (PDI) units at the  $\alpha$  position, allowing the most facile rotation of the PDI group

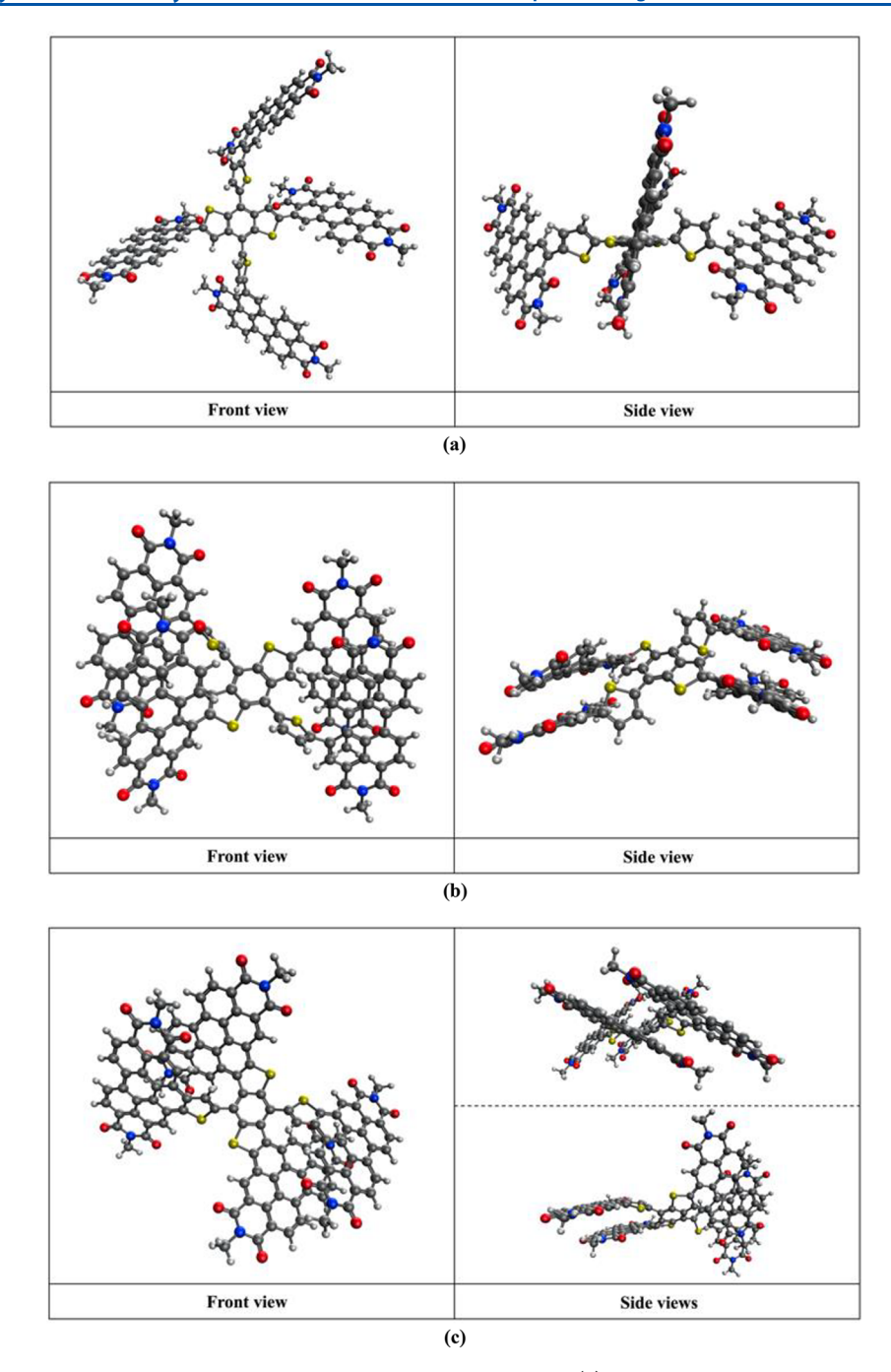


Figure 9. Ground-state optimized geometries of the tetramers considered in this work. (a) Ground-state optimized geometry of the  $\alpha$ -tetramer, (b) Ground-state optimized geometry of  $\beta$ . (c) Ground-state optimized geometry of  $\beta$ C.

with respect to the central unit. <sup>92</sup> As a result,  $\alpha$  has PDI units that are perpendicular to the central unit; this perpendicular orientation eliminates the possibility of  $\pi-\pi$  stacking between the individual PDI units. For the  $\beta$  molecule, the  $\beta$  positioning results in PDI units that pair off, with strong  $\pi-\pi$  stacking between two pairs of interacting PDIs. On the other hand, in the  $\beta$ C molecule, the PDI units are rigidly linked to the benzodithiophene (BDT) core, which results in greater coplanarity between the linker and PDI chromophores. These varying geometries among the investigated tetramers lead to differences in the electronic structure of the chromophores' excited states.

The natural transition orbitals (NTOs) for  $S_0 \rightarrow S_1$  transitions of the tetramers are shown in Figure 10. For  $\alpha$ ,

the  $S_0{\to}S_1$  NTOs are completely localized on a single PDI unit, suggesting low coupling between the PDI units, which is also supported by the steady-state measurements. The  $S_0{\to}S_1$  NTOs for  $\beta$  are slightly more delocalized with the electron density spread out to the central PDI linker and the adjacent PDI unit. This delocalization indicates some coupling between adjacent PDI units. However, for  $\beta C$ , the ease of  $\pi$ -conjugation across the coupled units enables the NTOs to be delocalized across most parts of the molecular structure. This delocalization also indicates the presence of a strong coupling among the PDI units in the rigidly bridged, planar tetrameric system. Using time-dependent DFT (TD-DFT) calculations and taking into account the solvation effects of chlorobenzene whose dielectric constant is 5.62,  $S_0{\to}S_1$  singlet energies of

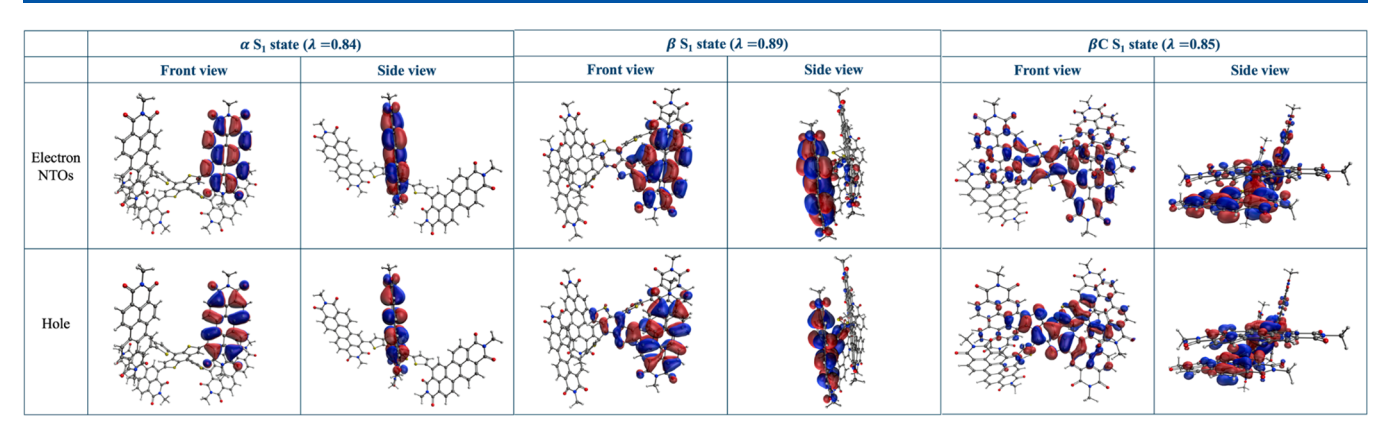


Figure 10. Natural transition orbitals (NTOs) of  $S_0 \rightarrow S_1$  transitions for the three tetramers considered in this work. Orbitals plotted in IQmol with an isovalue of 0.05.

Table 5. Single-Point Energies Calculated with  $\omega$ -B97XD Basis and Dielectric Constants of 5.62 for  $C_6H_5Cl$  (Chlorobenzene) and 2.38 for  $C_7H_8$  (Toluene) for the Investigated Tetramers<sup>a</sup>

	absolute $S_0 \rightarrow S_1$ energies		absolute $S_0 \rightarrow T_1$ energies		nergies	emission $S_1 \rightarrow S_0$ energies at $S_1$ geometry	emission $T_1 \rightarrow S_0$ experimental	
tetramers	C <sub>6</sub> H <sub>5</sub> Cl	$C_7H_8$	gas	C <sub>6</sub> H <sub>5</sub> Cl	$C_7H_8$	gas	gas	C <sub>6</sub> H <sub>5</sub> Cl
$\alpha$	2.90	2.91	3.02	1.76	1.76	1.76	1.06	2.31
β	2.55	2.55	2.61	1.63	1.64	1.64	0.87	2.21
$\beta$ C	2.91	2.92	2.95	2.05	2.05	2.05	1.43	2.21
<sup>a</sup> Energies are given in eV.								

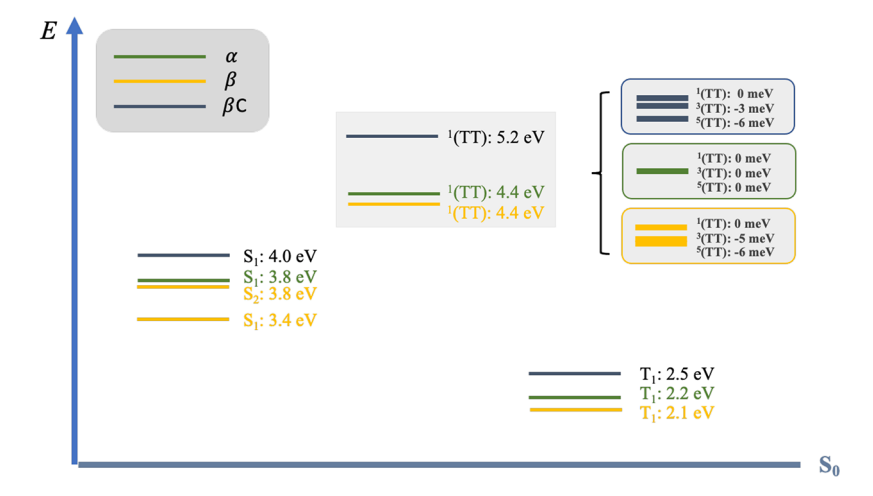


Figure 11. RAS-2SF results for the truncated tetramers. Due to the size limit of CI calculations, in the truncated model structure, only one pair of the adjacent PDI unit in each tetramer system is considered.

2.90 eV for the  $\alpha$ , 2.55 eV for the  $\beta$  and 2.91 eV for the  $\beta$ C (Table 5) were reported. From our steady-state measurements, it is clear that the singlet absorption energies  $(S_0 \rightarrow S_1)$  for both  $\alpha$  and  $\beta$  tetramers are identical while that of  $\beta$ C is blue-shifted (2.34, 2.34, and 2.46 eV for  $\alpha$ ,  $\beta$ , and  $\beta$ C, respectively). A similar trend is also expected for the TD-DFT calculations. While the TD-DFT method has been reported to overly estimate the singlet and triplet energies, the trend in these energies should match the experimental energies trend. This is not the case for the tetramers experimental results and TD-DFT calculations. The discrepancy may be as a result of the different functionals and basis sets used for the TD-DFT calculations or the fact that we are not sure that the calculated  $S_0 \rightarrow S_1$  energies are from the relaxed state. While a better comparison of singlet energies would be through the relaxed singlet state energies from the  $S_1 \rightarrow S_0$  emission, the large size of our molecules challenged our efforts to calculate these singlet emission energies using TD-DFT. These relaxed singlet energies would be expected to match those obtained from our steady-state emission (2.31 eV for the  $\alpha$ , 2.21 eV for the  $\beta$  and 2.21 eV for the  $\beta$ C).

Further quantum chemical simulations were performed to give insights into possible triplet formation mechanisms for the tetramers. In the  $\alpha$ -tetramer, the NTOs for the  $T_1$  states ( $S_0 \rightarrow T_1$  transition; Figure S34) are each localized on a single PDI. Time-dependent DFT (TD-DFT) calculations give adiabatic  $S_0 \rightarrow T_1$  triplet energies of 1.76 eV for the  $\alpha$ , 1.63 eV for the  $\beta$ , and 2.05 eV for the  $\beta$ C in chlorobenzene. For efficient iSEF, the lowest optically allowed singlet excited state  $[S_1]$  of the chromophore should have an excitation energy of at least twice its triplet energy:  $(E[S_1] > 2 \times E[T_1])$ . Considering the triplet and singlet absorption energies shown in Table 5, iSEF is

energetically uphill by 0.62 eV for the  $\alpha$ , 0.71 eV for the  $\beta$ , and 1.19 eV for the  $\beta$ C. This endothermic behavior shows that iSEF is not possible in any of the investigated chromophores.

In order to explore the accessibility of potential double triplet states (<sup>1</sup>[TT]), restricted active space spin flip (RAS-SF) was used to describe the character of multiexcitonic states (Figure 10 and Tables S3 and S4). To perform RAS-SF calculations for molecules with such large sizes, RAS-SF was performed on the "half" tetramers with only 2 PDI units (RAS-2SF), as shown in Figures S35-S38. Similar to the TD-DFT calculations, RAS-2SF is believed to overestimate the calculated energies in comparison to what is obtained experimentally. However, our RAS-2SF calculations shown in Figure 11 show that the singlet  $(S_1)$  energy for the  $\alpha$ -tetramer is 3.8 eV while that of the  $\beta$ -tetramer is 3.4 eV. This suggests that the RAS-2SF method error could be around  $\pm 0.4$  eV. Disregarding the  $\pm 0.4$  eV error observed in these S<sub>1</sub> energies, iSEF should be energetically uphill by 0.60 eV for  $\alpha$ , 0.80 eV for the  $\beta$ -tetramer, and by 1.0 eV for  $\beta$ C. These results are consistent with those obtained through our TD-DFT calculations. While this thermodynamic behavior is strange for iSEF materials, it has been reported that the production of independent triplets from a singlet becomes less endoergic as the molecular size increases. 93 For acene materials, this endothermic SEF behavior  $(2T_1 > S_1)$  is not new. The endothermic energy deficit  $(2T_1 - S_1)$  for these iSEF acene molecules has been reported to be 0.53 and 0.18 eV for anthracene and tetracene, respectively.1 Therefore, it is possible that some of our investigated molecules are eligible to undergo iSEF even after defying the thermodynamic conditions. In all three cases, the calculated energy for the double triplet <sup>1</sup>[TT] state is above the S<sub>1</sub>, which is also atypical. Similar energetics, where the <sup>1</sup>[TT] energy is higher than the S<sub>1</sub> energy, have been reported for PDI derivatives undergoing iSEF, with endothermic driving energies (<sup>1</sup>[TT] –  $S_1$ ) ranging from 0.2 to 1.05 eV.<sup>93</sup> From our RAS-2SF, the calculated endothermic driving energy is 0.614, 0.983, and 1.157 eV for  $\alpha$  ,  $\beta$ , and  $\beta$ C, respectively, with a probable error of  $\pm 0.57$  eV for each of these energy differences. The RAS-2SF energies provide insight about the feasibility of formation of the double triplet <sup>1</sup>[TT] state and separation of excitons from the <sup>1</sup>[TT] state into two independent triplets. Therefore, considering the endothermic energy drives from the RAS-2SF calculations,  $\alpha$  is likely to undergo iSEF compared to  $\beta$  and  $\beta$ C.

#### IV. DISCUSSION

Literature proposes that the presence of a  $\pi$ -bridge linker and its flexibility is important in triggering intramolecular singlet exciton fission (iSEF). <sup>26,38,53</sup> In this present investigation, we show that the  $\pi$ -bridge linker flexibility is necessary but not sufficient in activating iSEF in multichromophoric perylene diimide (PDI) systems. Here, we show the importance of the position of attachment of the PDI units to the core ( $\pi$ -bridge linker) in dendritic PDI tetramer systems. Owing to the flexibility of the  $\pi$ -bridge linker, the triplet energy is tuned such that the iSEF energetic criteria  $(E_{S1} \ge 2E_{T1})$  may be satisfied. In this work, key differences between  $\alpha$ - and  $\beta$ -functionalized flexible-bridged systems compared to a rigid-bridged  $\beta$ C system are pointed out as they relate to the efficiency and rate of triplet production upon photoexcitation. As an important result of our study, we demonstrate that, in addition to the conformational flexibility of the  $\pi$ -bridge linker, the position of functionalization on the PDI ( $\alpha$  and  $\beta$ ) and the

dielectric environment play a role in activating iSEF or excimer formation in these molecules.

We observe differences in the steady-state properties of the two flexible  $\pi$ -bridged systems. The steady absorption and emission spectra of  $\alpha$  in chlorobenzene show striking resemblance with the spectra of the parent PDI monomer. This indicates minimal excitonic coupling among its PDI units. This lack of coupling is further confirmed by the extinction coefficient of the  $\alpha$ , which is four (4x) times that of the parent PDI monomer. The relatively broad absorption spectrum with less vibronic structures of  $\beta$ , compared to that of  $\alpha$ , resembles the reported absorption spectra of prepared films of the PDI monomer. 94 The narrower, structured, and blue-shifted spectra of the rigid  $\pi$ -bridged  $\beta C$  system are expected for planar PDI molecules. 40,77 The  $\beta$ C absorption maxima is similar to that of a benzodithiophene (BDT) substitute. The similarities of  $\alpha$ and the PDI monomer surprisingly disappear upon comparing their fluorescence quantum yield in chlorobenzene. The fluorescence quantum yield for  $\alpha$  in chlorobenzene is four orders of magnitude (0.04%) lower than that of the parent PDI monomer (97%). The comparatively low quantum yield in  $\alpha$ suggests an alternative deactivation pathway that competes with the traditional radiative deactivation pathway of the photoexcited parent PDI monomer. However, in toluene, the emission spectra of  $\alpha$  have an additional broad peak centered around 710 nm and these spectra are concentration-dependent. In addition,  $\alpha$ 's fluorescence quantum yield increases significantly in toluene, matching that of  $\beta$  in toluene. Therefore, in toluene,  $\alpha$  has a tendency to form excimers as evidenced the above emission spectra characteristics, which inhibit iSEF. For  $\beta$ , the broad and red-shifted emission band at 710 nm, which happens to be concentration-dependent, points toward the formation of excimers for this compound in both chlorobenzene and toluene. The low fluorescence quantum yield of  $\alpha$ , as well as the observation of excimers in  $\beta$ , has been addressed using quantum chemical calculations and timeresolved measurements.

For  $\alpha$ , optimized ground-state geometries showed large perylene diimide-thiophene (PDI-Th) and perylene diimidebenzodithiophene-perylene diimide (PDI-BDT-PDI) angles of 78.7° and 63.5°, respectively. This nearly perpendicular connection between the two PDI units connected through the thiophene (Th), and the two PDI units connected through the BDT core indicate the twisted nature of this PDI tetramer system. The almost perpendicular orientation of the  $\alpha$ functionalized PDI units introduces a large steric hindrance between individual PDI units, minimizing their exciton coupling and creating a good separation between the orbitals in the PDI units of this molecule. As a result, it is expected that the photophysical characteristics of  $\alpha$  should resemble those of the parent PDI monomer. We observed that the  $\beta$ -position leads to PDI units that pair off in a co-facial orientation with a strong  $\pi$ – $\pi$  stacking between two pairs of interacting PDIs, an orientation that supports the formation of excimers.

The thermodynamic condition of iSEF is  $E[S_1] > 2 \times E[T_1]$ . Considering the singlet and triplet energies obtained through time-dependent density functional theory (TD-DFT), with chlorobenzene solvation effects factored in, iSEF is energetically uphill by 0.62 eV for  $\alpha$ , 0.71 eV for the  $\beta$ -tetramer and by 1.19 eV for  $\beta$ C. These results show that iSEF is thermodynamically impossible for all the investigated molecules. These results are consistent with those obtained from RAS-2SF where iSEF is energetically uphill by 0.60 eV for  $\alpha$ , 0.80 eV for the  $\beta$ -

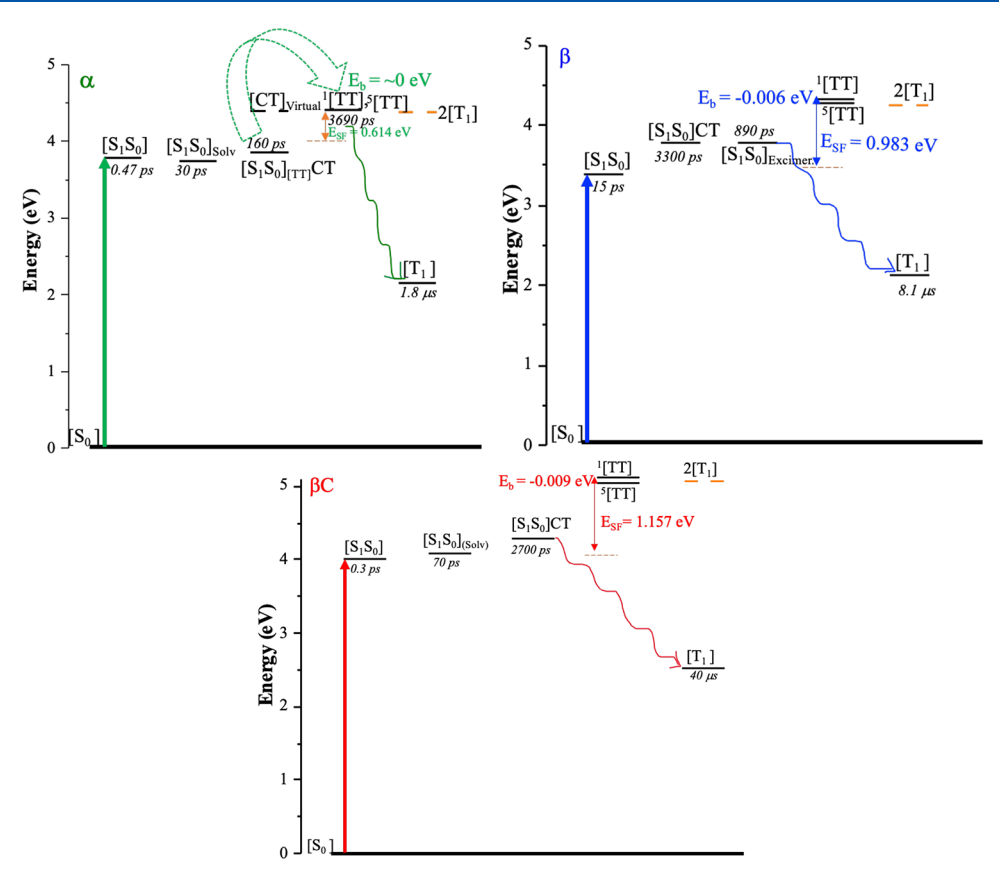


Figure 12. Proposed singlet deactivation and triplet formation pathways for the investigated PDI tetramers in chlorobenzene from our RAS-2SF.

tetramer, and by 1.0 eV for  $\beta$ C. The thermodynamic rule has been defied by singlet exciton fission materials, anthracene and tetracene, with an endothermic energy deficit reported to be 0.53 and 0.18 eV, respectively, where singlet fission is thermally activated.7 The endothermic fission was used to explain the extremely low fluorescence quantum yield of tetracene since singlet fission was the dominant deactivation pathway for the singlets. St is therefore possible that the  $\alpha$  compound, whose energy deficit is close to that of anthracene, is capable of showing iSEF. On the other hand, using the calculated  $T_1 \rightarrow S_0$ emission energies (1.06 eV for the  $\alpha$ , 0.87 eV for the  $\beta$ , and 1.46 eV for the  $\beta$ C) together with our experimental relaxed  $S_1 \rightarrow S_0$  energies (2.31 eV for the  $\alpha$ , 2.21 eV for the  $\beta$ , and 2.21 eV for  $\beta$ C), we notice that iSEF is energetically favorable for the  $\alpha$  by 0.21 eV and 0.52 eV for the  $\beta$  but energetically uphill for  $\beta$ C by 0.57 eV (Figure S39). From these calculations, iSEF is thermodynamically viable for both  $\alpha$  and  $\beta$ . However, for the parent PDI monomer, iSEF thermodynamic requirement is not fulfilled owing to its reported triplet (~1.2 eV) and singlet (2.34 eV) energies. 96

On the other hand, using the RAS-2SF to predict the iSEF kinetic feasibility, surprisingly, shows that among the three investigated tetramers, only the  $\alpha$ -functionalized chromophore has the possibility of undergoing iSEF. We use a model by Farag et al., <sup>93</sup> which defines the factors affecting the rates of the individual steps in the iSEF process. The rate of formation of the  $^1[TT]$  from the  $S_1$  (first step) depends on the energy drive  $(E_{SF})$  and the nonadiabatic coupling (NAC) between these two states as described in detail in the literature. <sup>45,93,97</sup> On the other hand, the rate of the second step depends on the multiexciton binding energy  $(E_b)$ . This multiexcitonic interaction quantifies the charge transfer contributions to the

singlet multiexcitonic states, compared to the pure quintet multiexcitonic states. From our RAS-2SF calculations of truncated molecules, we find that the  $E_{\rm SF}$  for  $\alpha$  is 0.614 eV, as shown in Figure 12. This  $E_{\rm SF}$  is lower compared to that of  $\beta$ (0.983 eV) and  $\beta$ C (1.148 eV), indicating that singlet fission would be more probable in the  $\alpha$ -tetramer. Using the same RAS-2SF calculations, we determine the modified binding energy,  $E_{\rm b}$ , for all the investigated chromophores. Unlike  $\beta$  and  $\beta$ C tetramers, there is negligible multiexcitonic interaction energy ( $\sim 0$  eV) for the  $\alpha$  system, where the <sup>1</sup>[TT] state is degenerate with its corresponding quintet <sup>5</sup>[TT] state. This zero coupling between the two excitons leads to an easy separation of the entangled excitons to form the two independent triplets since, for weakly interacting triplet pairs, only a small activation energy is required to spatially separate the triplets. The  $E_h$  for  $\beta$  and  $\beta$ C are -0.006 and -0.009 eV, respectively. Thus, no additional energy is required for the two triplets to be separated in  $\alpha$ , whereas in  $\beta$  and  $\beta$ C systems, this step requires more energy as shown in Figure 11. This lower binding energy for  $\alpha$  indicates that the energy penalty to decouple the double triplet state into two separated triplets is negligible, making the second step of singlet fission possible for this molecule compared to  $\beta$  and  $\beta$ C. Overall, the RAS-2SF calculations reveal that iSEF is kinetically feasible for  $\alpha$ , making this molecule a possible candidate for iSEF. The trend of  $E_{\rm SF}$ and  $E_{\rm b}$  obtained for our molecules is consistent with those previously obtained for PDI dimers. 93 The location of the  $^{1}[TT]$  state above the  $S_{1}$  state shows that the  $E_{SF}$  for our PDI tetramers is endoergic and leads to iSEF for the  $\alpha$ . Therefore, it is possible that the negligible fluorescence quantum yield obtained for  $\alpha$  is a result of the nonradiative pathway due to the accessibility of the double triplet state in this molecule. The iSEF thermodynamic disparities observed in these molecules and the conflicting iSEF kinetic feasibility for the  $\alpha$  compound call for a detailed analysis of the time-resolved spectroscopic measurements to not only confirm the compound undergoing iSEF but also explore the iSEF mechanism. This analysis would also be used to explain the absence of iSEF in  $\beta$  despite the molecule showing energy levels similar to those of  $\alpha$ .

With our time-resolved measurements, we were able to confirm iSEF in only one of the flexible  $\pi$ -bridged compounds,  $\alpha$  in chlorobenzene. For this flexible  $\alpha$ -functionalized chromophore, we observe a triplet yield of 126% using our nanosecond sensitization experiments and a fast triplet formation of 160 ps with the femtosecond transient absorption (fsTA) technique. Our findings suggest that iSEF takes place in  $\alpha$  upon photoexcitation for which its thermodynamic and kinetic viability is predicted by quantum chemical simulations. Interestingly, the long-lived independent triplets are experimentally observed following their separation, and each of them is localized on a single PDI of the tetramer, as shown in the results of the theoretical calculations. This is really interesting as long-lived triplet excitons are indeed required for efficient solar energy conversion. We use a previous iSEF model by Wasielewski and Guldi<sup>29</sup> to explain iSEF in  $\alpha$  as a quantum coherent mechanism. For the  $\alpha$  in chlorobenzene, and as shown in Figure 12, we propose that optical excitation populates the  $[S_1S_0]$  state, which then populates the  ${}^1[TT]$ through electronic coupling to  $[S_1S_0]$ . Due to the closeness in energy, coherent electronic coupling among the CT state, the [S<sub>1</sub>S<sub>0</sub>] and <sup>1</sup>[TT] form a coherent quantum superposition state:  $[S_1S_0]_{[TT]}CT$ . This superposition state then loses coupling immediately (within 160 ps), forming the double triplet state (1[TT]). The second step of iSEF follows where the spin coherence of <sup>1</sup>[TT] is lost, and the correlated double triplet state dephases to form two independent triplets and hence high fission yield in  $\alpha$ . Recent improvements in the field of singlet fission show that despite energetic inconsistencies, this fission process can still proceed endoergically due to entropic contributions. 48 Therefore, even though  $\alpha$  does not fulfil the thermodynamic requirements for singlet fission, we propose that the strong electronic coherent coupling between the molecule's  $[S_1S_0]$ , the CT and the  ${}^1[TT]$  states enable the singlet excitons to access the endothermic multiexcitonic state. In addition, the entropic gains mainly acquired through the excitonic interaction with its environment enables the singlet excitons to overcome the thermodynamic energy barrier and proceed through the production of the double triplet states, <sup>1</sup>[TT], and dephasing of these <sup>1</sup>[TT] to form independent triplet states (iSEF).

In  $\beta$ , the expected iSEF (upon satisfying the thermodynamic condition) is hindered by strong excimer formation. For this  $\beta$ -functionalized flexible system, we observe a low triplet quantum yield and slow triplet formation. Additionally, our quantum chemical calculations show that the  $\beta$  natural transition orbitals (NTOs) are highly delocalized and the electron density spreads out from the central BDT linker to the adjacent PDI units. This strong delocalization supports increased coupling between opposite PDI units of  $\beta$  compared to those of  $\alpha$ . This behavior is due to the formation of intermediate excimer states, which act as traps, competing with internal conversion to the double triplet state. Our experimental evidence for the excimer formation in  $\beta$  include (i) broad, red-shifted emission, (ii) concentration-dependent emission as previously observed, was a supported to the satisfactory of the excimer formation of the emission as previously observed, was a supported to the excimer formation of the emission as previously observed, was a supported to the excimer formation of the emission as previously observed, was a supported to the excimer formation of the emission as previously observed, was a supported to the excimer formation of the emission as previously observed, was a supported to the excimer formation of the

fluorescence decay lifetimes, and (iv) co-facial  $\pi$ - $\pi$  stacking of the PDI units in the optimized geometry. These excimer species are observed in  $\alpha$  when the polarity of the environment is lowered (in toluene). For  $\alpha$  in toluene, we observe a concentration-dependent emission, a slower singlet decay and triplet formation (380 ps), and a triplet quantum yield of only 61%. These observations are due to the decreased viscosity of the solvent, which has been observed to increase the ratio of the excimer to the monomer. Due to the minimal coupling observed between the opposite PDI units of  $\alpha$ chromophore, its molecular structure is subject to perturbations due to the solvation effects, and this could explain the formation of excimer states in this molecule in toluene. In summary, the deactivation pathway of photoexcited singlets in  $\beta$  and  $\alpha$  in toluene is not via iSEF (regardless of satisfying the iSEF thermodynamic condition) as there is strong competition with excimer formation, which trap singlet excitons preventing the formation of the <sup>1</sup>[TT] state.

Although all the investigated molecules are charge transfer molecules, we observe the highest two-photon absorption (TPA) cross section in  $\beta$ C. This suggests the presence of a non-radiative singlet deactivation pathway and fluorescence quenching caused by intramolecular charge transfer (iCT). The rigidity and enhanced planarity of  $\beta$ C leads to a stronger iCT character. We find that triplet production for the rigid  $\beta$ C tetramer proceeds via intersystem crossing because we observe triplet yields lower than 30% and slow triplet formation occurring in few nanoseconds ( $\sim$ 2 ns).

The crucial properties affecting multiexciton generation clearly emerge in comparing the photobehavior of the flexible  $\pi$ -bridged systems,  $\beta$  and  $\alpha$ . Although both  $\alpha$  and  $\beta$  are highly twisted, the  $\alpha$ -functionalized PDI units are completely isolated and do not show any interaction with each other nor with the BDT core while the  $\beta$ -substituted units arrange in a co-facial stacked structure. As a result, the absorption and emission spectra of the  $\alpha$  resembles those of the parent PDI monomer; this lack of coupling permits efficient iSEF. On the contrary, the  $\beta$ -substitution of the core increases the coupling between the PDI chromophores, leading them to have a co-facial  $\pi$ - $\pi$  interaction and therefore allowing the formation of excimers. These intermediate excimer states trap the localized Frenkel excitons, thus preventing singlet exciton fission into the correlated triplet pair.

#### V. CONCLUSIONS

In this study, crucial properties affecting multiexciton generation clearly emerge in comparing the photobehavior of three analogous PDI tetramers showing flexible ( $\alpha$  and  $\beta$ ) and rigid ( $\beta$ C)  $\pi$ -bridge linker, as well as their parent PDI monomer. The steady-state spectral and computational results of the  $\alpha$ -tetramer suggest very minimal interaction among the individual PDI units. However, while the reported fluorescence quantum yield for the parent PDI monomer is close to unity, that of the  $\alpha$  compound is negligible, indicating the presence of a nonradiative decay pathway for this compound. Our TD-DFT and RAS-2SF calculations predict that intramolecular singlet exciton fission (iSEF) is thermodynamically impossible for all the investigated molecules. However, the triplet quantum yields obtained through triplet sensitization experiments are 124% and 17% for  $\alpha$  and  $\beta$  compounds, respectively. In addition, our femtosecond transient absorption shows an ultrafast triplet formation for  $\alpha$  (160 ps). Therefore, we have solid experimental evidence of iSEF only in the  $\alpha$ -tetramer in

chlorobenzene. Our RAS-2SF calculations show that, among the studied tetramers,  $\alpha$  has the lowest  $[S_1S_0] - {}^1[TT]$  energy gap, indicating the highest rate of forming the <sup>1</sup>[TT] state. In addition, the energy penalty for this <sup>1</sup>[TT] to dissociate into independent triplets is ~0 eV for this molecule, making it possible to complete the second step of iSEF. We suggest that this <sup>1</sup>[TT] state is formed from a superposition of singlet states known as  $[S_1S_0]_{[TT]}CT$ , which is made possible through the increased coherent coupling, while the entropic energy drive necessitates the dephasing of the <sup>1</sup>[TT] into independent triplet states. The absence of iSEF in the other twisted  $\pi$ bridged compound,  $\beta_1$  is due to the production of excimers following photoexcitation. These excimer states act as singlet exciton traps inhibiting the formation of the double triplet states. Similarly, for  $\alpha$  in a less polar solvent, we observe the formation of excimers and a subsequent reduction of the triplet quantum yield (61%). For the rigid  $\beta$ C tetramer, the main singlet deactivation pathway is through intramolecular charge transfer (iCT) and a small triplet production was observed (24%) via intersystem crossing. The flexibility of the linker has previously been demonstrated as an important factor in triggering iSEF. In this present investigation, we show that the linker flexibility is necessary but not sufficient in activating iSEF in multichromophoric systems. As an important result of our study, we demonstrate that, in addition to the conformational flexibility of the linker, the position of attachment of the core to the PDI units the surrounding medium play a role in driving iSEF or excimer formation in these dendritic molecules.

#### ASSOCIATED CONTENT

#### Supporting Information

The Supporting Information is available free of charge at https://pubs.acs.org/doi/10.1021/acs.jpcb.1c02534.

Concentration effects on the absorption spectra of the investigated tetramers in chlorobenzene; global analysis of the femtosecond transient absorption and triplet yield calculation from the femtosecond transient absorption data; triplet energy sensitization and relative actinometry experiments done using nanosecond transient absorption; and additional quantum chemical simulations (PDF)

#### AUTHOR INFORMATION

#### **Corresponding Author**

Theodore Goodson, III — Department of Chemistry, University of Michigan, Ann Arbor, Michigan 48109, United States; orcid.org/0000-0003-2453-2290; Email: tgoodson@umich.edu

#### **Authors**

Angelar K. Muthike – Department of Chemistry, University of Michigan, Ann Arbor, Michigan 48109, United States

Benedetta Carlotti — Department of Chemistry Biology and Biotechnology, University of Perugia, 06123 Perugia, Italy; orcid.org/0000-0002-2980-2598

Ifeanyi K. Madu — Department of Chemistry, University of Michigan, Ann Arbor, Michigan 48109, United States; orcid.org/0000-0003-3576-1427

 Hanjie Jiang – Department of Chemistry, University of Michigan, Ann Arbor, Michigan 48109, United States
 Hyungjun Kim – Department of Chemistry, University of Michigan, Ann Arbor, Michigan 48109, United States; Department of Chemistry, Incheon National University, Incheon 22012, Republic of Korea; orcid.org/0000-0002-7204-3718

Qinghe Wu – Department of Chemistry and The James Franck Institute, The University of Chicago, Chicago, Illinois 60637, United States

Luping Yu — Department of Chemistry and The James Franck Institute, The University of Chicago, Chicago, Illinois 60637, United States

Paul M. Zimmerman — Department of Chemistry, University of Michigan, Ann Arbor, Michigan 48109, United States;
orcid.org/0000-0002-7444-1314

Complete contact information is available at: https://pubs.acs.org/10.1021/acs.jpcb.1c02534

#### Notes

The authors declare no competing financial interest.

### ACKNOWLEDGMENTS

T.G. III would like to thank the Department of Energy, Basic Energy Sciences (DE-SC0020168) and the U.S. Air Force Office of Scientific Research in the Biophysics program via F058689 for support of this research. B.C. acknowledges support from the Italian "Ministero per l'Università e la Ricerca Scientifica e Tecnologica", MIUR (Rome, Italy) under the "Dipartimenti di Eccellenza 2018–2022" (grant AMIS) program. L.Y. acknowledges the NSF (Chem-1802274, LPY) for their support in this work.

# REFERENCES

- (1) Smith, M. B.; Michl, J. Recent advances in singlet fission. *Annu. Rev. Phys. Chem.* **2013**, *64*, 361–386.
- (2) Shockley, W.; Queisser, H. J. Detailed balance limit of efficiency of p-n junction solar cells. *J. Appl. Phys.* **1961**, *32*, 510–519.
- (3) Hanna, M. C.; Nozik, A. J. Solar conversion efficiency of photovoltaic and photoelectrolysis cells with carrier multiplication absorbers. *J. Appl. Phys.* **2006**, *100*, No. 074510.
- (4) Rao, A.; Friend, R. H. Harnessing Singlet Exciton Fission to Break the Shockley-Queisser Limit. Nat. Rev. Mater. 2017, 2, 17063.
- (5) Smith, M. B.; Michl, J. Singlet fission. Chem. Rev. 2010, 110, 6891–6936.
- (6) Greyson, E. C.; Stepp, B. R.; Chen, X.; Schwerin, A. F.; Paci, I.; Smith, M. B.; Akdag, A.; Johnson, J. C.; Nozik, A. J.; Michl, J.; et al. Singlet Exciton Fission for Solar Cell Applications: Energy Aspects of Interchromophore Coupling. *J. Phys. Chem. B* **2010**, *114*, 14223–14232.
- (7) Zimmerman, P. M.; Zhang, Z.; Musgrave, C. B. Singlet Fission in Pentacene through Multi-Exciton Quantum States. *Nat. Chem.* **2010**, 2, 648–652.
- (8) Zimmerman, P. M.; Bell, F.; Casanova, D.; Head-Gordon, M. Mechanism for Singlet Fission in Pentacene and Tetracene: From Single Exciton to Two Triplets. *J. Am. Chem. Soc.* **2011**, *133*, 19944–19952.
- (9) Chan, W. L.; Berkelbach, T. C.; Provorse, M. R.; Monahan, N. R.; Tritsch, J. R.; Hybertsen, M. S.; Reichman, D. R.; Gao, J.; Zhu, X. Y. The Quantum Coherent Mechanism for Singlet Fission: Experiment and Theory. *Acc. Chem. Res.* **2013**, *46*, 1321–1329.
- (10) Monahan, N.; Zhu, X. Y. Charge Transfer-Mediated Singlet Fission. *Annu. Rev. Phys. Chem.* **2015**, *66*, 601–618.
- (11) Berkelbach, T. C.; Hybertsen, M. S.; Reichman, D. R. Microscopic Theory of Singlet Exciton Fission. I. General Formulation. *J. Chem. Phys.* **2013**, *138*, 114102.
- (12) Berkelbach, T. C.; Hybertsen, M. S.; Reichman, D. R. Microscopic Theory of Singlet Exciton Fission. II. Application to

- Pentacene Dimers and the Role of Superexchange. J. Chem. Phys. 2013, 138, 114103.
- (13) Fuemmeler, E. G.; Sanders, S. N.; Pun, A. B.; Kumarasamy, E.; Zeng, T.; Miyata, K.; Steigerwald, M. L.; Zhu, X. Y.; Sfeir, M. Y.; Campos, L. M.; et al. A Direct Mechanism of Ultrafast Intramolecular Singlet Fission in Pentacene Dimers. *ACS Cent. Sci.* **2016**, *2*, 316–324.
- (14) Low, J. Z.; Sanders, S. N.; Campos, L. M. Correlating Structure and Function in Organic Electronics: From Single Molecule Transport to Singlet Fission. *Chem. Mater.* **2015**, 27, 5453–5463.
- (15) Varnavski, O.; Abeyasinghe, N.; Arago, J.; Serrano-Perez, J. J.; Ortí, E.; Lopez Navarrete, J. T.; Takimiya, K.; Casanova, D.; Casado, J.; et al. High Yield Ultrafast Intramolecular Singlet Exciton Fission in a Quinoidal Bithiophene. *J. Phys. Chem. Lett.* **2015**, *6*, 1375–1384.
- (16) Miller, C. E.; Wasielewski, M. R.; Schatz, G. C. Modeling Singlet Fission in Rylene and Diketopyrrolopyrrole Derivatives: The Role of the Charge Transfer State in Superexchange and Excimer Formation. *J. Phys. Chem. C* **2017**, *121*, 10345–10350.
- (17) Miyata, K.; Kurashige, Y.; Watanabe, K.; Sugimoto, T.; Takahashi, S.; Tanaka, S.; Takeya, J.; Yanai, T.; Matsumoto, Y. Coherent Singlet Fission Activated by Symmetry Breaking. *Nat. Chem.* **2017**, *9*, 983–989.
- (18) Basel, B. S.; Zirzlmeier, J.; Hetzer, C.; Reddy, S. R.; Phelan, B. T.; Krzyaniak, M. D.; Volland, M. K.; Coto, P. B.; Young, R. M.; Clark, T.; et al. Evidence for Charge-Transfer Mediation in the Primary Events of Singlet Fission in a Weakly Coupled Pentacene Dimer. Chem 2018, 4, 1092–1111.
- (19) Korovina, N. V.; Das, S.; Nett, Z.; Feng, X.; Joy, J.; Haiges, R.; Krylov, A. I.; Bradforth, S. E.; Thompson, M. E. Singlet Fission in a Covalently Linked Cofacial Alkynyltetracene Dimer. *J. Am. Chem. Soc.* **2016**, *138*, *6*17.
- (20) Mandal, A.; Chen, M.; Foszcz, E.; Schultz, J. D.; Kearns, N. M.; Young, R. M.; Zanni, M. T.; Wasielewski, M. R. Two Dimensional Electronic Spectroscopy Reveals Excitation Energy Dependent State Mixing during Singlet Fission in a Terrylenediimide Dimer. *J. Am. Chem. Soc.* **2018**, *140*, 17907–17914.
- (21) Basel, B. S.; Zirzlmeier, J.; Hetzer, C.; Phelan, B. T.; Krzyaniak, M. D.; Reddy, S. R.; Coto, P. B.; Horwitz, N. E.; Young, R. M.; White, F. J.; et al. Unified Model for Singlet Fission within a Non-conjugated Covalent Pentacene Dimer. *Nat. Commun.* **2016**, *8*, 1–8.
- (22) Hong, Y.; Kim, J.; Kim, W.; Kaufmann, C.; Kim, H.; Würthner, F.; Kim, D. Efficient Multiexciton State Generation in Charge-Transfer Coupled Perylene Bisimide Dimers via Structural Control. *J. Am. Chem. Soc.* **2020**, *142*, 7845–7857.
- (23) Stern, H. L.; Cheminal, A.; Yost, S. R.; Broch, K.; Bayliss, S. L.; Chen, K.; Tabachnyk, M.; Thorley, K.; Greenham, N.; Hodgkiss, J. M.; et al. Vibronically Coherent Ultrafast Triplet-Pair Formation and Subsequent Thermally Activated Dissociation Control Efficient Endothermic Singlet Fission. *Nat. Chem.* **2017**, *9*, 1205.
- (24) Greyson, E. C.; Vura-Weis, J.; Michl, J.; Ratner, M. A. Maximizing Singlet Fission in Organic Dimers: Theoretical Investigation of Triplet Yield in the Regime of Localized Excitation and Fast Coherent Electron Transfer. J. Phys. Chem. B 2010, 114, 14168.
- (25) Krishnapriya, K. C.; Musser, A. J.; Patil, S. Molecular Design Strategies for Efficient Intramolecular Singlet Exciton Fission. ACS Energy Lett. 2019, 4, 192.
- (26) Korovina, N. V.; Joy, J.; Feng, X.; Feltenberger, C.; Krylov, A. I.; Bradforth, S. E.; Thompson, M. E. Linker-Dependent Singlet Fission in Tetracene Dimers. J. Am. Chem. Soc. 2018, 140, 10179.
- (27) Huang, H.; He, G.; Xu, K.; Wu, Q.; Wu, D.; Sfeir, M. Y.; Xia, J. Achieving Long-Lived Triplet States in Intramolecular SF Films through Molecular Engineering. *Chem* **2019**, *5*, 2405.
- (28) Sanders, S. N.; Kumarasamy, E.; Pun, A. B.; Appavoo, K.; Steigerwald, M. L.; Campos, L. M.; Sfeir, M. Y. Exciton Correlations in Intramolecular Singlet Fission. *J. Am. Chem. Soc.* **2016**, *138*, 7289.
- (29) Papadopoulos, I.; Zirzlmeier, J.; Hetzer, C.; Bae, Y. J.; Krzyaniak, M. D.; Wasielewski, M. R.; Clark, T.; Tykwinski, R. R.;

- Guldi, D. M. Varying the Interpentacene Electronic Coupling to Tune Singlet Fission. *J. Am. Chem. Soc.* **2019**, *141*, 6191.
- (30) Alvertis, A. M.; Lukman, S.; Hele, T. J. H.; Fuemmeler, E. G.; Feng, J.; Wu, J.; Greenham, N. C.; Chin, A. W.; Musser, A. J. Switching between Coherent and Incoherent Singlet Fission via Solvent-Induced Symmetry Breaking Dimer. J. Am. Chem. Soc. 2019, 141. 17558.
- (31) Weiss, L. R.; Bayliss, S. L.; Kraffert, F.; Thorley, K. J.; Anthony, J. E.; Bittl, R.; Friend, R. H.; Rao, A.; Greenham, N. C.; Behrends, J. Strongly Exchange-Coupled Triplet Pairs in an Organic Semi-conductor. *Nat. Phys.* **2017**, *13*, 176.
- (32) Conrad-Burton, F. S.; Liu, T.; Geyer, F.; Costantini, R.; Schlaus, A. P.; Spencer, M. S.; Wang, J.; Sanchez, R. H.; Zhang, B.; Xu, Q.; et al. Controlling Singlet Fission by Molecular Contortion. *J. Am. Chem. Soc.* **2019**, *141*, 13143.
- (33) Rickhaus, M.; Mayor, M.; Juríček, M. Strain-Induced helical Chirality in Polyaromatic Systems. *Chem. Soc. Rev.* **2016**, *45*, 1542–1556.
- (34) Maliakal, A.; Raghavachari, K.; Katz, H.; Chandross, E.; Siegrist, T. Photochemical Stability of Pentacene and a Substituted Pentacene in Solution and in Thin Films. *Chem. Mater.* **2004**, *16*, 4980.
- (35) Hartnett, P. E.; Timalsina, A.; Matte, H. R.; Zhou, N.; Guo, X.; Zhao, W.; Facchetti, A.; Chang, R. P.; Hersam, M. C.; Wasielewski, M. R.; et al. Slip-Stacked Perylenediimides as an Alternative Strategy for High Efficiency Nonfullerene Acceptors in Organic Photovoltaics. *J. Am. Chem. Soc.* **2014**, *136*, 16345–16356.
- (36) Chen, W.; Zhang, Q. Recent Progress in Non-Fullerene Small Molecule Acceptors in Organic Solar Cells (Oscs). *J. Mater. Chem. C* **2017**, *5*, 1275–1302.
- (37) Würthner, F.; Saha-Möller, C. R.; Fimmel, B.; Ogi, S.; Leowanawat, P.; Schmidt, D. Perylene Bisimide Dye Assemblies as Archetype Functional Supramolecular Materials. *Chem. Rev.* **2016**, *116*, 962–1052.
- (38) Margulies, E. A.; Miller, C. E.; Wu, Y.; Ma, L.; Schatz, G. C.; Young, R. M.; Wasielewski, M. R. Enabling Singlet Fission by Controlling Intramolecular Charge Transfer in Π-Stacked Covalent Terrylenediimide Dimers. *Nat. Chem.* **2016**, *8*, 1120–1125.
- (39) Schierl, C.; Niazov-Elkan, A.; Shimon, L. J. W.; Feldman, Y.; Rybtchinski, B.; Guldi, D. M. Singlet Fission in Self-Assembled PDI Nanocrystals. *Nanoscale* **2018**, *10*, 20147.
- (40) Carlotti, B.; Madu, I. K.; Zimmerman, P.; Muthike, A. K.; Jiang, H.; Cai, Z.; Yu, L.; Kim, H.; Goodson, T., III Activating Intramolecular Singlet Exciton Fission by Altering  $\pi$  Bridge Flexibility in Perylene diimide Trimers for Organic Solar Cells. *Chem. Sci.* **2020**, *11*, 8757—8770.
- (41) Margulies, E. A.; Shoer, L. E.; Eaton, S. W.; Wasielewski, M. R. Excimer Formation in Cofacial and Slip-Stacked Perylene-3,4:9,10-Bis(Dicarboximide) Dimers on a Redox-Inactive Triptycene Scaffold. *Phys. Chem. Chem. Phys.* **2014**, *16*, 23735–23742.
- (42) Brown, K. E.; Salamant, W. A.; Shoer, L. E.; Young, R. M.; Wasielewski, M. R. Direct Observation of Ultrafast Excimer Formation in Covalent Perylenediimide Dimers Using Near-Infrared Transient Absorption Spectroscopy. *J. Phys. Chem. Lett.* **2014**, *5*, 2588–2593.
- (43) Lefler, K. M.; Brown, K. E.; Salamant, W. A.; Dyar, S. M.; Knowles, K. E.; Wasielewski, M. R. Triplet State Formation in Photoexcited Slip-Stacked Perylene-3,4:9,10-Bis(Dicarboximide) Dimers on a Xanthene Scaffold. *J. Phys. Chem. A* **2013**, *117*, 10333.
- (44) Lindquist, R. J.; Lefler, K. M.; Brown, K. E.; Dyar, S. M.; Margulies, E. A.; Young, R. M.; Wasielewski, M. R. Energy Flow Dynamics Within Cofacial and Slip-Stacked Perylene-3,4- Dicarboximide Dimer Models of P-Aggregates. *J. Am. Chem. Soc.* **2014**, *136*, 14192–14923.
- (45) Feng, X.; Krylov, A. I. On Couplings And Excimers: Lessons from Studies of Singlet Fission in Covalently Linked Tetracene Dimers. *Phys. Chem. Chem. Phys.* **2016**, *18*, 7751–7761.
- (46) Johnson, J. C.; Nozik, A. J.; Michl, J. The Role of Chromophore Coupling in Singlet Fission. *Acc. Chem. Res.* **2013**, *46*, 1290–1299.

- (47) Feng, X.; Luzanov, A. V.; Krylov, A. I. Fission of Entangled Spins: An Electronic Structure Perspective. *J. Phys. Chem. Lett.* **2013**, 4, 3845–3852.
- (48) Kolomeisky, A. B.; Feng, X.; Krylov, A. I. A Simple Kinetic Model for Singlet Fission: A Role of Electronic and Entropic Contributions to Macroscopic Rates. *J. Phys. Chem. C* **2014**, *118*, 5188–5195.
- (49) Liu, H.; Nichols, V. M.; Shen, L.; Jahansouz, S.; Chen, Y.; Hanson, K. M.; Bardeen, C. J.; Li, X. Synthesis and Photophysical Properties of a "Face-To-Face" Stacked Tetracene Dimer. *Phys. Chem. Chem. Phys.* **2015**, *17*, 6523–6531.
- (50) Katoh, R.; Sinha, S.; Murata, S.; Tachiya, M. Origin of the Stabilization Energy of Perylene Excimer as Studied by Fluorescence and Near-IR Transient Absorption Spectroscopy. *J. Photochem. Photobio. A* **2001**, *145*, 23–34.
- (51) Mauck, C. M.; Hartnett, E. A.; Mergulies, E. A.; Ma, L.; Miller, C. E.; Schatz, G. C.; Marks, T. J.; Wasielewski, M. R. Singlet Fission via an Excimer-Like Intermediate in 3,6-Bis(Thiophen-2-Yl) Diketopyrrolopyrrole Derivatives. *J. Am. Chem. Soc.* **2016**, *138*, 11749.
- (52) Young, R. M.; Wasielewski, M. R. Mixed Electronic States in Molecular Dimers: Connecting Singlet Fission, Excimer Formation, and Symmetry-Breaking Charge Transfer. *Acc. Chem. Res.* **2020**, 1120–1125.
- (53) Yamakado, T.; Takahashi, S.; Watanabe, K.; Matsumoto, Y.; Osuka, A.; Saito, S. Conformational Planarization Versus Singlet Fission: Distinct Excited State Dynamics of Cyclooctatetraene Fused Acene Dimers. *Angew. Chem., Int. Ed.* **2018**, *57*, 5438–5443.
- (54) Chen, M.; Bae, Y. J.; Mauck, C. M.; Mandal, A.; Young, R. M.; Wasielewski, M. R. Singlet Fission in Covalent Terrylenediimide Dimers: Probing the Nature of the Multiexciton State Using a Femtosecond Mid-Infrared Spectroscopy. *J. Am. Chem. Soc.* **2018**, 140, 9184.
- (55) Lukman, S.; Musser, A. J.; Chen, K.; Athanasopoulos, S.; Yong, C. K.; Zeng, Z.; Ye, Q.; Chi, C.; Hodgkiss, J. M.; Wu, J.; et al. Tuneable Singlet Exciton Fission and Triplet-Triplet Annihilation in an Orthogonal Pentacene Dimer. *Adv. Funct. Mater.* **2015**, 25, 5452–5461
- (56) Tayebjee, M. J. Y.; Sanders, S. N.; Kumarasamy, E.; Campos, L. M.; Sfeir, M. Y.; McCamey, D. R. Quintet Multiexciton Dynamics in Singlet Fission. *Nat. Phys.* **2017**, *13*, 182.
- (57) Wu, Q.; Zhao, D.; Schneider, A. M.; Chen, W.; Yu, L. Covalently Bound Clusters of Alpha-Substituted PDI-Rival Electron Acceptors to Fullerene for Organic Solar Cells. *J. Am. Chem. Soc.* **2016**, *138*, 7248–7251.
- (58) Wu, Q.; Zhao, D.; Yang, J.; Sharapov, V.; Cai, Z.; Li, L.; Zhang, N.; Neshchadin, A.; Chen, W.; Yu, L. Propeller Shaped Acceptors for High Performance Non Fullerene Solar Cells: Importance of the Rigidity of Molecular Geometry. *Chem. Mater.* **2017**, *29*, 1127–1133.
- (59) McLean, A. M.; Socher, E.; Varnavski, O.; Clark, T. B.; Imperiali, B.; Goodson, T., III Two-Photon Fluorescence Spectroscopy and Imaging of 4-Dimethylaminonaphthalimide Peptide and Protein Conjugates. *J. Phys. Chem. B* **2013**, *117*, 15935–15942.
- (60) Beaumont, P. C.; Johnson, D. G.; Parsons, B. J. Photophysical Properties of Laser Dyes: Picosecond Laser Flash Photolysis Studies of Rhodamine 6G, Rhodamine B and Rhodamine 101. *J. Chem. Soc., Faraday Trans.* **1993**, *89*, 4185–4191.
- (61) Keller, B.; Cai, Z.; Muthike, A. K.; Sahu, P. K.; Kim, H.; Eshun, A.; Zimmerman, P. M.; Zhang, D.; Goodson, T., III Investigating the Optical Properties of Thiophene Additions to s-Indacene Donors with Diketopyrrolopyrrole, Isoindigo, and Thienothiophene Acceptors. *J. Phys. Chem. C* **2018**, *122*, 27713–27733.
- (62) Vázquez, R. J.; Kim, H.; Zimmerman, P. M.; Goodson, T., III Using Ultrafast Spectroscopy to Probe the Excited State Dynamics of a Reported Highly Efficient thermally Activated Delated Fluorescence Chromophore. *J. Mater. Chem. C* **2019**, *7*, 4210–4221.
- (63) Vázquez, R.; Yun, J. H.; Muthike, A. K.; Howell, M.; Kim, H.; Madu, I. K.; Kim, T.; Zimmerman, P.; Lee, J. Y.; Goodson, T., III New Direct Approach for Determining the Reverse Intersystem

- Crossing Rate in Organic Thermally Activated Delayed Fluorescent (TADF) Emitters. J. Am. Chem. Soc. 2020, 142, 8074–8079.
- (64) Murov, S. L.; Carmichael, I.; Hug, G.L. Handbook of Photochemistry, 2nd Edition, Marcel Dekker, Inc., New York, 1993.
- (65) Chai, J.-D.; Head-Gordon, M. Long-Range Corrected Hybrid Density Functionals with Damped Atom-Atom Dispersion Corrections. *Phys. Chem. Chem. Phys.* **2008**, *10*, 6615–6620.
- (66) Chai, J. D.; Head-Gordon, M. Systematic Optimization of Long Range Corrected Hybrid Density Functionals. *J. Chem. Phys.* **2008**, *128*, No. 084106.
- (67) Mewes, J. M.; Herbert, J. M.; Dreuw, A. On the Accuracy of the General, State-Specific Polarizable-Continuum Model for the Description of Correlated Ground-And Excited States in Solution. *Phys. Chem. Chem. Phys.* **2017**, *19*, 1644–1654.
- (68) Chien, A. D.; Molina, A. R.; Abeyasinghe, N.; Varnavski, O. P.; Goodson, T., III; Zimmerman, P. M. Structure and Dynamics of the 1 (TT) State in a Quinoidal Bithiophene: Characterizing a Promising Intramolecular Singlet Fission Candidate. *J. Phys. Chem. C* **2015**, *119*, 28258–28268.
- (69) Rudenko, A. E.; Clayman, N. E.; Walker, K. L.; Maclaren, J. K.; Zimmerman, P. M.; Waymouth, R. M. Ligand-Induced Reductive Elimination of Ethane from Azopyridine Palladium Dimethyl Complexes. J. Am. Chem. Soc. 2018, 140, 11408–11415.
- (70) Kim, H.; Keller, B.; Ho-Wu, R.; Abeyasinghe, N.; Vázquez, R. J.; Goodson, T., III; Zimmerman, P. M. Enacting Two-Electron Transfer from a Double-Triplet State of Intramolecular Singlet Fission. *J. Am. Chem. Soc.* **2018**, *140*, 7760–7763.
- (71) Kim, H.; Zimmerman, P. M. Coupled Double Triplet State in Singlet Fission. *Phys. Chem. Chem. Phys.* **2018**, *20*, 30083–30094.
- (72) Jiang, H.; Zimmerman, P. M. Charge Transfer Via Spin Flip Configuration Interaction: Benchmarks and Application to Singlet Fission. *J. Chem. Phys.* **2020**, *153*, 164109.
- (73) Shao, Y.; Gan, Z.; Epifanovsky, E.; Gilbert, A. T. B.; Wormit, M.; Kussmann, J.; Lange, A. W.; Behn, A.; Deng, J.; Feng, X.; et al. Advances in Molecular Quantum Chemistry Contained in the Q-Chem 4 Program Package. *Mol. Phys.* **2015**, *113*, 184–215.
- (74) Schaftenaar, G.; Noordik, J. H. Molden: A Pre-And Post-Processing Program for Molecular find Electronic Structures. *J. Comput.-Aided Mol. Des.* **2000**, *14*, 123.
- (75) Humphrey, W.; Dalke, A.; Schulten, K. VMD: Visual Molecular Dynamics. *J. Mol. Graph.* **1996**, *14*, 33–38.
- (76) Le, A. K.; Bender, J. A.; Arias, D. H.; Cotton, D. E.; Johnson, J. C.; Roberts, S. T. Singlet Fission Involves an Interplay between Energetic Driving Force and Electronic Coupling in Perylenediimide Films. J. Am. Chem. Soc. 2018, 140, 814–826.
- (77) Carlotti, B.; Cai, Z.; Kim, H.; Shaparov, V.; Madu, I. K.; Zhao, D.; Chen, W.; Zimmerman, P. M.; Yu, L.; Goodson, T., III Charge Transfer and Aggregation Effects in the Performance of Planar vs. Twisted Perylene Diimide Isomers as Electron Acceptors in Organic Solar Cells. *Chem. Mater.* **2018**, *30*, 4263–4276.
- (78) Longhi, E.; Bossi, A.; Di Carlo, G.; Maiorana, S.; De Angelis, F.; Salvatori, P.; Petrozza, A.; Binda, M.; Roiati, V.; Mussini, P. R.; et al. Metal-free benzodithiophene-containing organic dyes for dyesensitized solar cells. *Eur. J. Org. Chem.* **2013**, 84–94.
- (79) Cai, Z.; Vázquez, R. J.; Zhao, D.; Li, L.; Lo, W. Y.; Zhang, N.; Wu, Q.; Keller, B.; Eshun, A.; Abeyasinghe, N.; et al. Two photon absorption study of low-bandgap, fully conjugated perylene diimidethienoacene-perylene diimide ladder-type molecules. *Chem. Mater.* 2017, 29, 6726–6732.
- (80) Yong, C. K.; Musser, A. J.; Bayliss, S. L.; Lukman, S.; Tamura, H.; Bubnova, O.; Hallani, R. K.; Meneau, A.; Resel, R.; Maruyama, M.; et al. The Entangled Triplet Pair State in Acene and Heteroacene Materials. *Nat. Commun.* **2017**, *8*, 1–12.
- (81) Roberts, S. T.; McAnally, R. E.; Mastron, J. N.; Webber, D. H.; Whited, M. T.; Brutchey, R. L.; Thompson, M. E.; Bradforth, S. E. Efficient Singlet Fission Discovered in a Disordered Acene Film. *J. Am. Chem. Soc.* **2012**, *134*, 6388–6400.
- (82) Spenst, P.; Young, R. M.; Wasielewski, M. R.; Wurthner, F. Guest and Solvent Modulated Photo-Driven Charge Separation and

- Triplet Generation in a Perylene Bismide Cyclophane. *Chem. Sci.* **2016**, *7*, 5428–5434.
- (83) Brown, K. E.; Veldkamp, B. S.; Co, D. T.; Wasielewski, M. R. Vibrational Dynamics of a Perylene–Perylenediimide Donor–Acceptor Dyad Probed with Femtosecond Stimulated Raman Spectroscopy. J. Phys. Chem. Lett. 2012, 3, 2362–2366.
- (84) Fron, E.; Pilot, R.; Schweitzer, G.; Qu, J.; Herrmann, A.; Mullen, K.; Hofkens, J.; Van der Auweraer, M.; De Schryver, F. C. Photoinduced Electron Transfer in Perylenediimide Triphenylamine—Based Dendrimers: Single Photon Timing and Femtosecond Transient Absorption Spectroscopy. *Photochem. Photobiol. Sci.* 2008, 7, 597–604.
- (85) Giaimo, J. M.; Gusev, A. V.; Wasielewski, M. R. Excited State Symmetry Breaking in Cofacial and Linear Dimers of a Green Perylenediimide Chlorophyll Analogue Leading to Ultrafast Charge Separation. J. Am. Chem. Soc. 2002, 124, 8530–8531.
- (86) Van der Boom, T.; Hayes, R. T.; Zhao, Y.; Bushard, P. J.; Weiss, E. A.; Wasielewski, M. R. Charge Transport in Photofunctional Nanoparticles Self–Assembled from Zinc 5,10,15,20–Tetrakis–(perylenediimide)porphyrin Building Blocks. *J. Am. Chem. Soc.* 2002, 124, 9582–9590.
- (87) Lukas, A. S.; Zhao, Y.; Miller, S. E.; Wasielewski, M. R. Biomimetic Electron Transfer Using Low Energy Excited States: A Green Perylene Based Analogues of Chlorophyll a. *J. Phys. Chem. B* **2002**, *106*, 1299–1306.
- (88) Sung, J.; Nowak Krol, A.; Schlosser, F.; Fimmel, B.; Kim, W.; Kim, D.; Wurthner, F. Direct Observation of Excimer Mediated Intramolecular Electron Transfer in a Cofacially Stacked Perylene Bisimide Pair. J. Am. Chem. Soc. 2016, 138, 9029–9032.
- (89) Guo, Y.; Ma, Z.; Niu, X.; Zhang, W.; Tao, M.; Guo, Q.; Wang, Z.; Xia, A. Bridge-Mediated Charge Separation in Isomeric N-Annulated Perylene Diimide Dimers. *J. Am. Chem. Soc.* **2019**, *141*, 12789–12796.
- (90) Montero, R.; Martínez-Martínez, V.; Longarte, A.; Epelde-Elezcano, N.; Palao, E.; Lamas, I.; Manzano, H.; Agarrabeitia, A. R.; López Arbeloa, I.; Ortiz, M. J.; et al. Singlet fission mediated photophysics of bodipy dimers. *J. Phys. Chem. Let.* **2018**, *9*, 641–646.
- (91) Ford, W. E.; Kamat, P. V. Photochemistry of 3, 4, 9, 10-perylenetetracarboxylic dianhydride dyes. 3. Singlet and triplet excited-state properties of the bis (2, 5-di-tert-butylphenyl) imide derivative. *J. Phys. Chem.* **1987**, *91*, 6373–6380.
- (92) Shen, L.; Chen, Y.; Li, X.; Gao, J. Effects of Substituents on Tetracene Derivatives on their Stabilities and Singlet Fission. *J. Mol. Graphics Modell.* **2014**, *51*, 86–96.
- (93) Farag, M. H.; Krylov, A. I. Singlet Fission in Perylenediimide Dimers. J. Phys. Chem. C 2018, 122, 25753–25763.
- (94) Abd-Ellah, M.; Cann, J.; Dayneko, S. V.; Laventure, A.; Cieplechowicz, E.; Welch, G. C. Interfacial ZnO Modification Using a Carboxylic Acid Functionalized N-Annulated Perylene Diimide for Inverted Type Organic Photovoltaics. *ACS Appl. Electron. Mater.* **2019**, *1*, 1590–1596.
- (95) Groff, R. P.; Avakian, P.; Merrifield, R. E. Coexistance of exciton fission and fusion in tetracene crystals. *Phys. Rev. B* **1970**, *1*, 815
- (96) Eaton, S. W.; Shoer, L. E.; Karlen, S. D.; Dyar, S. M.; Margulies, E. A.; Veldkamp, B. S.; Ramanan, C.; Hartzler, D. A.; Savikhin, S.; Marks, T. J.; et al. Singlet Exciton Fission in Polycrystalline Thin Films of a Slip-Stacked Perylenediimide. *J. Am. Chem. Soc.* **2013**, *135*, 14701–14712.
- (97) Feng, X.; Kolomeisky, A. B.; Krylov, A. I. Dissecting the Effect of Morphology on the Rates of Singlet Fission: Insights from Theory. *J. Phys. Chem. C* **2014**, *118*, 19608–19617.
- (98) Zhao, D.; Wu, Q.; Cai, Z.; Zheng, T.; Chen, W.; Lu, J.; Yu, L. Electron Acceptors Based on  $\alpha$ -Substituted Perylene Diimide (PDI) for Organic Solar Cells. *Chem. Mater.* **2016**, 28, 1139–1146.
- (99) Walker, B. J.; Musser, A. J.; Beljonne, D.; Friend, R. H. Singlet exciton fission in solution. *Nat. Chem.* **2013**, *5*, 1019–1024.

- (100) Nishihara, T.; Kaneko, M. The Dependence of Excimer Formation of Polystyrene Solutions on Solvent and Concentration. *Macromol. Chem. Phys.* **1969**, *124*, 84–90.
- (101) Snare, M. J.; Thistlethwaite, P. J.; Ghiggino, K. P. Kinetic Studies of Intramolecular Excimer Formation in Dipyrenylalkanes. *J. Am. Chem. Soc.* **1983**, *105*, 3328–3332.
- (102) Diaz, C.; Vesga, Y.; Echevarria, L.; Stará, I. G.; Starỳ, I.; Anger, E.; Shen, C.; Moussa, M. E. S.; Vanthuyne, N.; Crassous, J.; et al. Two-Photon Absorption and Two-Photon Circular Dichroism of Hexahelicene Derivatives: A Study of the Effect of the Nature of Intramolecular Charge Transfer. RSC Adv. 2015, 5, 17429–17437.